Journal of Mining and Environment (JME) Vol. 17, No. 2, 2026, 717-742

Shahrood University of Technology

Journal of Mining and Environment (JME)

Journal homepage: www.jme.shahroodut.ac.ir

Iranian Society of Mining Engineering (IRSME)

Numerical Modeling of Hydraulic Fracturing for Crack Growth Mechanism Investigation in Rocks Using XFEM with A BEM-Based Verification

Mohammad Reza Zeerak[1], Mohammad Fatehi Marji[1*], Manouchehr Sanei[1], Mehdi Najafi[1], and Abolfazl Abdollahipour[2]

1. Department of Mining and Metallurgical Engineering, Yazd University, Yazd, Iran
2. School of Mining Engineering, College of Engineering, University of Tehran, Tehran, Iran

Article Info

Received 27 February 2025
Received in Revised form 7 April 2025
Accepted 20 April 2025
Published online 20 April 2025

DOI: 10.22044/jme.2025.15836.3047

Keywords

Extended finite element method
Hydraulic fracturing
Crack orientation and growth
Boundary element method
Rock fracture mechanics

Abstract

The Extended Finite Element Method (XFEM) is a leading computational approach for studying crack growth in rocks, as it can effectively model complex crack paths and discontinuities without the need for re-meshing. In this context, XFEM is particularly well-suited for simulating the development of hydraulic fractures. XFEM is employed to investigate crack initiation, propagation, and aperture size in rock formations, with validation using a Boundary Element Method (BEM)-based approach. Three scenarios are analyzed for crack orientation and interaction in: single cracks at 0°, 15°, 30°, and 60°; crack displacement behavior at 15° and 60°; multiple cracks at 60° and 120°. Displacement in the vertical direction (U2) and stress distribution around the crack tip in the S22 direction are examined to understand fracture mechanics parameters. The findings highlight that crack at higher angles, such as 120°, exhibit more straightforward propagation, while those at or beyond 90° often require additional stress to continue growing. The comparison between XFEM and BEM results confirms the reliability of the numerical approach, demonstrating strong agreement in predicting fracture behavior in rock materials. The results provide deeper insights into fracture evolution, stress intensity factors, and fracture toughness in geological media. These simulations advance computational fracture mechanics, contributing to optimizing hydraulic fracturing techniques for improved efficiency and safety in subsurface formations. This study is limited to 2D geometries and isotropic materials, potentially missing 3D heterogeneous subsurface complexities. Future work could explore 3D models, anisotropy, and fluid pressure/thermal effects to improve crack growth predictions.

1. Introduction

Hydraulic fracturing (HF) is a primary technique for stimulating tight formations with very low permeability, enabling the extraction of oil and gas from unconventional reservoirs. The first attempt to fracture a well dates back to 1864, when Edward Augustus Leonard Roberts used dynamite and nitroglycerin in a well, a method known as the highly dangerous torpedo technology. Even a small mistake during the fracturing operation can result in severe injury or death. The widespread use of hydraulic fracturing began in 1949, when J.B. Clark published a paper on well stimulation using the hydraulic process with Stanolind Oil and Gas Company. This process involves injecting viscous fluids with proppants to create fractures in the formation, reducing the viscosity of injected fluids before production begins. The first successful HF operation occurred in 1953 in southern Oklahoma and North Central Texas. Horizontal drilling and multi-stage hydraulic fracturing are two important techniques for the development of unconventional reservoirs

Corresponding author: mfatehi@yazd.ac.ir (M. Fatehi Marji)

[1]. By creating multiple transverse fractures in a horizontal well, fewer vertical wells are required to achieve the same number of fractures. As shown in Figure 1, a horizontal well is capable of creating multiple fractures and significantly enhancing the single random variable method, which helps produce much more oil or gas compared to a vertical well. However, the stress shadow effect may prevent some fractures from growing in a horizontal well. Production from the remaining fractures helps save on the cost of drilling new vertical wells [2].

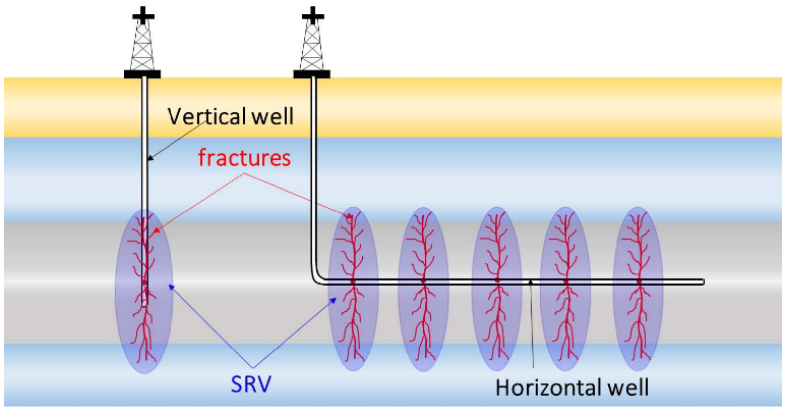

Figure 1. Hydraulic fracturing in a vertical and a horizontal well [2].

However, it was not until the early 1980s that commercial breakthroughs in horizontal well drilling were achieved by the French oil company Elf Aquitaine [2]. In 2003, the commercial success rate of horizontal well drilling in the United States was approximately 65% [3]. By 2004, only 15% of the crude oil in the United States was produced from low-permeability formations using horizontal wells. The main factor hindering horizontal well drilling programs may be the high risk involved. With improvements in drilling technology for unconventional reservoirs, production accelerated from 2008, and by the end of 2018, over 96% of crude oil and gas production in the United States from unconventional reservoirs was produced by horizontal wells [4]. Over the years, advancements in hydraulic fracturing techniques have been critical for tapping into unconventional reservoirs, and accurate modeling of crack initiation and propagation has become essential [5].

Numerous researchers have examined hydraulic fracturing both in field conditions and during controlled experiments. These studies have provided valuable insights into the behavior and geometry of fractures in oil wells. By utilizing specialized packers and capturing images with cameras, the geometry of fractures along the wellbore walls can be observed and documented. Below, the studies conducted by several researchers in the field of hydraulic fracturing are highlighted. Companies conducting or planning hydraulic fracturing in Australia include Santos, Origin Energy, Arrow Energy, Westside Corporation, AGL, Queensland Gas Company, and a joint venture between Origin Energy, ConocoPhillips, and Sinopec. Data from APPEA (2013) shows that 1,844 coal seam gas wells (including 1,341 exploratory wells and 3,731 production wells) were drilled in Australia over 15 months from April 2012 to June 2013, with 111 of them (6%) involving hydraulic fracturing. DEHP (2013d) estimates that in Queensland, this proportion could increase to 10–40% with the expansion of the industry [6].

G. Zielonka et al. (2014) developed and validated new Abaqus capabilities for simulating hydraulically driven fractures in porous, permeable media. Using coupled pressure/deformation cohesive elements and XFEM-based enriched elements, they modeled fracturing fluid flow, porous medium deformation, and fracture propagation. These results confirm Abaqus' readiness for hydraulic fracturing applications such as injection, stimulation, and drilling in the oil and gas industry [7]. Guo et al. (2015), developed a cohesive-zone finite-element model to simulate interactions between hydraulic fractures (HF) and natural fractures (NF) without requiring crossing criteria. The study analyzed how factors such as in-situ stress, approaching angle, and NF cementing strength influence fracture geometries. Results showed that lower approaching angles and smaller differential stresses facilitate NF activation and propagation, contributing to complex fracture networks [8]. Kim et al. (2015) conducted numerical simulations on fracture propagation

during hydraulic fracturing in shale gas reservoirs. The study revealed that tensile fractures propagate discontinuously, causing saw-toothed pressure, aperture, and displacement responses. High intrinsic permeability facilitated rapid fracturing, while a strong geological layer limited vertical propagation by redirecting fractures horizontally. These findings emphasize the complex relationship between fluid dynamics, geomechanics, and geological conditions in hydraulic fracturing [9]. Ren et al. (2016) developed a fully coupled XFEM-EDFM model to simulate geomechanics and multiphase flow interactions in fractured tight gas reservoirs. The model uses an implicit time-stepping strategy and incorporates a proppant model to account for hydraulic fracture deformation during production. Validation against Mandel's problem and fracture mechanics scenarios confirmed its accuracy. The study revealed the significant influence of geomechanics on production, showing that neglecting stress-dependent effects leads to inaccurate predictions [10].

M. Yaylaci. (2016) in the study titled "The investigation crack problem through numerical analysis" conducted a comparative study between the finite element method (FEM) and analytical solutions for a layered composite with an internal perpendicular crack. The composite consisted of two elastic layers with different elastic properties, subjected to external loading via a rigid punch, while the lower layer was supported at both ends. Numerical analysis was performed using ANSYS software. The study focused on evaluating the normal stress $\sigma_x(0, y)$, stress intensity factors (SIFs), and crack opening displacements, and the results showed good agreement with existing analytical solutions [11]. Abdollahipour et al. (2018) studied the behavior of hydraulic fracturing in permeable formations using the poroelastic displacement discontinuity method to investigate the effect of permeability on hydraulic fracture development in formations with different permeabilities. The results showed that hydraulic fracture propagation can be significantly delayed in formations with permeability lower than Darcy's. The effect of fracture spacing on the propagation path was also examined. It was found that the stress shadow effect of hydraulic fractures, due to the time required for fluid leakage into the formation, remains significant over a longer distance compared to the elastic model [12]. Chen et al. (2018) developed a 3D solid-fluid coupled model to study hydraulic fracture growth in multiple horizontal wells. Key findings include the impact of inter-well stress interference, which causes asymmetric fracture propagation and suppresses lateral growth of interior fractures. Limited entry design promotes lateral propagation but is less effective with closely spaced wells. The study suggests maintaining a critical minimum well spacing to avoid adverse interference and resource waste. These insights aid in optimizing multi-well fracturing designs [13].

M. Yaylaci et al. (2022) in the study titled "Implementation of finite element and artificial neural network methods to analyze the contact problem of a functionally graded layer containing crack" analyzed the contact problem of a functionally graded layer (FGM) with a crack using both Finite Element Method (FEM) and Artificial Neural Networks (ANN). The research aimed to evaluate the impact of various geometric parameters and material properties on the crack behavior in such layers. The study showed that using FEM and ANN together can provide efficient solutions to complex crack and contact problems, highlighting the potential of these methods in solving issues similar to those in hydraulic fracture modeling [14]. M. Yaylaci. (2022) in the study titled, "Simulate of edge and internal crack problem and estimation of stress intensity factor through finite element method" examined the elastic plane problem of a layered composite with an internal or edge crack using the Finite Element Method (FEM). The layered composite consisted of two layers with different elastic properties, resting on a homogeneous elastic half-plane, and subjected to pressure from a rigid cylindrical stamp. The study found that the FEM results for the stress intensity factor (SIF) were in perfect agreement with analytical solutions from the literature. The effects of various geometric and material parameters on the SIF were discussed, showing that FEM can be an efficient alternative to analytical methods when applied correctly [15].

M. Yaylaci et al. (2023) used FEM and multi-layer perceptron (MLP) method for analysing the vibration and buckling in functionally graded material (FGM) beam with edge crack. They studied the effects of crack location (c/L), material properties (E_2/E_1), slenderness ratio (L/h) and end supports on the bending vibration and buckling properties of cracked FGM beam [16]. Zeerak et al. (2023) studied the "Investigating Hydraulic Fracture Models for Production Enhancement from Unconventional Hydrocarbon Reservoirs". The studies shows that hydraulic fracturing is a crucial technique for enhancing oil and gas extraction from

wells, particularly in unconventional reservoirs. The study provided a comprehensive review of numerical models used for simulating hydraulic fracturing, comparing various methods based on their advantages and disadvantages [17]. The study "Finite Element Analysis of Ratcheting on Beam under Bending-Bending Loading Conditions" by S. Fuyad et al. (published in 2023) investigates ratcheting in a cantilever beam under bending-loads using finite element analysis. It explores the effects of primary and secondary stresses and frequency on ratcheting onset, which can lead to plastic deformation, collapse, or fatigue, proposing a dimensionless ratcheting diagram that highlights worse conditions at lower frequencies and examines material modeling impact [18]. Fatehi Marji et al. (2023) studied the explosive fracturing technique to improve permeability and productivity in low-permeable reservoirs. They simulated crack initiation and propagation using explosions, with shock waves playing a key role in creating radial cracks around the wellbore. These cracks, filled with pressurized gas, further propagated in the reservoir rock. The study concluded that this explosive fracturing mechanism can significantly enhance the productivity of low-permeable reservoirs in horizontal wells [19]. A. Benouis et al. (2024) in the paper titled "Finite element analysis of the behavior of elliptical cracks emanating from the orthopedic cement interface in total hip prostheses" examined crack behavior in orthopedic cement used in total hip prostheses. They employed the Finite Element Method (FEM) to calculate stress intensity factors (SIF) near the crack tip under static and dynamic loading conditions. The analysis was conducted for cracks originating at the interface between cement and bone during activities such as regular walking, climbing stairs, and descending stairs. The study concluded that cracks emanating from the micro-interface under substantial loading can lead to cement damage and ultimately prosthetic loosening [20]. Yazdani et al. (2025) studied the impact of hydraulic fracturing on sand production in low-strength reservoirs, such as sandstone. Using a two-dimensional model in PFC2D software, they simulated three scenarios based on the fracture length relative to the well radius. Their findings showed that hydraulic fracturing significantly affects sand production rates, highlighting the importance of understanding this interaction to optimize reservoir recovery and ensure well integrity [21].

Previous studies have extensively examined hydraulic fracturing using various numerical techniques, such as finite element methods, cohesive zone modeling, and displacement discontinuity approaches. These studies primarily focused on fracture interaction, permeability effects, and stress shadow influence. However, a detailed investigation into the influence of crack orientation on fracture evolution has remained limited. Additionally, while many models have been validated using experimental data, benchmarking against numerical methods like BEM remains underexplored. This study aims to bridge these gaps by analyzing crack initiation, propagation patterns, and stress intensity variations in different fracture configurations. Given the lack of comprehensive numerical studies on angle-dependent crack growth behavior, this research focuses on modeling and validation using a boundary-based approach.

The objective of this study is to simulate fracture evolution in rocks during hydraulic fracturing using the XFEM and validate its accuracy with the BEM. Three fracture configurations are analyzed: (1) a single crack with specific orientations relative to the horizontal axis, (2) the effect of crack angle on fracture formation and propagation, and (3) a complex system of multiple interacting cracks. XFEM provides an advanced approach for modeling crack propagation without re-meshing, while BEM offers high precision in boundary problem solutions. By evaluating stress intensity factors, crack opening displacement, and interaction effects, this study contributes to improving numerical modeling in hydraulic fracturing. The ultimate goal is to enhance fracture mechanics simulations and improve the accuracy of crack behavior predictions by identifying optimal crack angles for enhanced permeability in rocks [22].

2. Linear Elastic Fracture Mechanics in XFEM

These concepts encompass the fundamental principles of linear elastic fracture mechanics, which are essential for understanding the behavior of materials under loading and stress. Elasticity is examined as the primary property of materials that deform under loading and return to their original shape upon unloading. Additionally, linearity is described as an assumption valid for many elastic materials, where deformation is directly proportional to the applied stress.

2.1. Stress Intensity Factor

The stress intensity factor (SIF) plays a basic role in the practical application of linear elastic

fracture mechanics (LEFM) principles. It enables the calculation of crack growth rates under conditions such as fatigue loading, stress corrosion, and others. For safety assessment, two critical factors are required: the SIF related to the applied load on the component and the material's fracture toughness. In analytical methods, the stress intensity factors for Modes I, II, and III are calculated using the following equations, provided that the stress field at the crack tip is expressed in terms of (r) and (θ) [23].

$$K_I = \lim_{r\to 0}\sqrt{2\pi r}\left(\sigma_y\right)_{\theta=0} \quad (1)$$

$$K_{II} = \lim_{r\to 0}\sqrt{2\pi r}\left(\tau_{xy}\right)_{\theta=0} \quad (2)$$

$$K_{III} = \lim_{r\to 0}\sqrt{2\pi r}\left(\tau_{yz}\right)_{\theta=0} \quad (3)$$

In all these scenarios, the crack tip serves as the origin, with the x-axis ($\theta = 0$) aligned along the crack plane and indicating the direction of crack propagation (Figure 2).

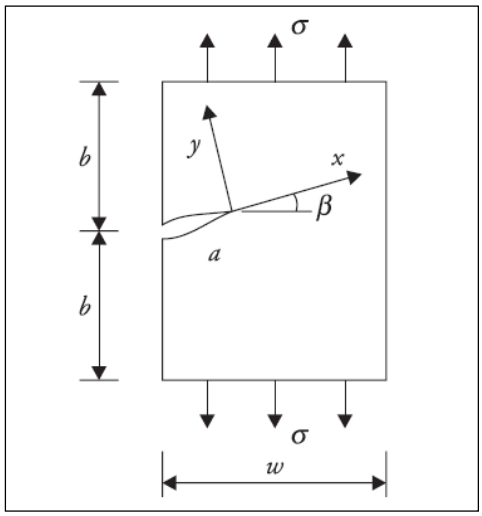

Figure 2. Plate with angled crack and crack-tip coordinates [23].

Below the SIF for several common geometries presents in the Table 1.

Table 1. Stress intensity factors for several common geometries [24]

Type of crack	SIF K_I
Center crack, length $2a$, in an infinite plate	$\sigma_\infty\sqrt{\pi a}$
Edge crack ,length a, in a semi-infinite plate	$1.12\sigma_\infty\sqrt{\pi a}$
Central penny-shaped crack, radius *a*, in infinite body	$2\sigma_\infty\sqrt{\frac{a}{\pi}}$
Center crack, length $2a$ in plate of width *W*	$\sigma_\infty\sqrt{W\tan\left(\frac{\pi a}{W}\right)}$
2 symmetrical edge cracks, each length a, in plate of total width *W*	$\sigma_\infty\sqrt{W\left[\tan\left(\frac{\pi a}{W}\right)+0.1\sin\left(\frac{2\pi a}{W}\right)\right]}$

2.2. Crack Deformation Modes

Pre-existing cracks in rock propagate under tensile and compressive loads, merge with each other, and form fracture planes. Many researchers have studied the initiation and propagation of cracks in brittle materials such as rocks with pre-existing cracks under various loading conditions [25]. For a specific crack under different loading conditions, crack propagation may occur in opening mode (Mode-I), shear mode (Mode-II), and tearing mode (Mode-III) (Figure 3) [26].

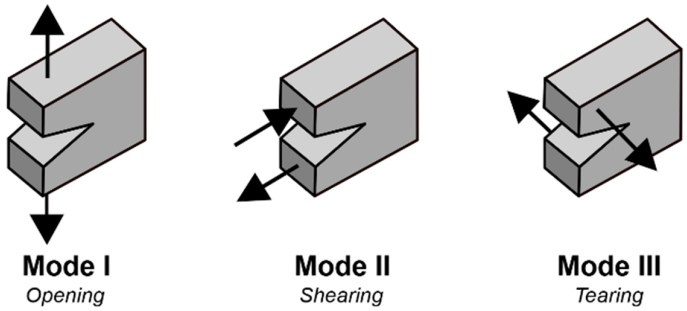

Figure 3. Modes of crack propagation: (I) Opening mode, (II) Shear mode, (III) Tearing mode [27].

In practice, the cracking of engineering structures usually occurs under mixed-mode loading (opening-shear mode). In mixed-mode conditions, both Mode-I and Mode-II stress intensity factors are nonzero. Using Irwin's LEFM theory, these factors represent the resistance of a brittle material to the crack propagation mechanism with a length of (l) from its tip (Figure 4). Irwin presented the following equations for stresses and stress intensity factors in the plane [26].

$$\sigma_{xx}=\frac{K_I}{\sqrt{2\pi r}}\cos\frac{\theta}{2}\left(1-\sin\frac{\theta}{2}\sin\frac{3\theta}{2}\right)-\frac{K_{II}}{\sqrt{2\pi r}}\sin\frac{\theta}{2}\left(2+\cos\frac{\theta}{2}\cos\frac{3\theta}{2}\right) \quad (4)$$

$$\sigma_{yy}=\frac{K_I}{\sqrt{2\pi r}}\cos\frac{\theta}{2}\left(1+\sin\frac{\theta}{2}\sin\frac{3\theta}{2}\right)+\frac{K_{II}}{\sqrt{2\pi r}}\sin\frac{\theta}{2}\cos\frac{\theta}{2}\cos\frac{3\theta}{2} \quad (5)$$

$$\tau_{xy}=\frac{K_I}{\sqrt{2\pi r}}\sin\frac{\theta}{2}\cos\frac{\theta}{2}\cos\frac{3\theta}{2}+\frac{K_{II}}{\sqrt{2\pi r}}\cos\frac{\theta}{2}\left(1-\sin\frac{\theta}{2}\sin\frac{3\theta}{2}\right) \quad (6)$$

Here $K=3-4v$ represents plane strain conditions, and $K=(3-v)/(1+v)$ indicates plane stress conditions.

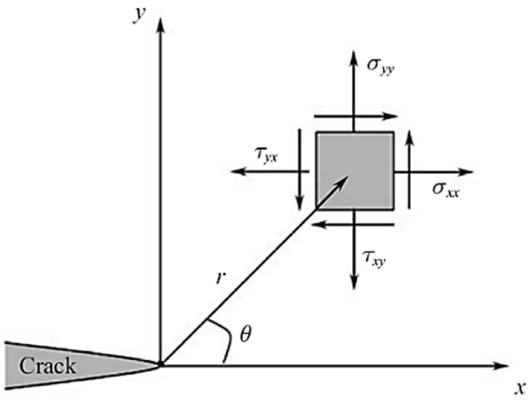

Figure 4. The coordinate system adjacent to the crack tip in two-dimensional deformation [26].

In hydraulic fracture modeling, fracture criteria are used to determine crack propagation, and the selection of these criteria largely depends on the numerical method employed. In discrete fracture modeling, LEFM and the cohesive zone model are commonly used. The LEFM method includes maximum tensile stress, minimum strain energy density, maximum principal strain, and maximum strain energy release criteria. Among these, the maximum tensile stress criterion is the most widely used, and it can be expressed as follows [26]:

$$\cos\frac{\theta}{2}\left(K_I\cos^2\frac{\theta}{2}-\frac{3}{2}K_{II}\sin\theta\right)\geq K_{Ic} \quad (7)$$

Where (K_I, K_{II}) and (K_{II}) are the stress intensity factors for Mode I, Mode II fracture, and fracture toughness, respectively, and the direction of propagation is as follows [26]:

$$\tan\left(\frac{\theta}{2}\right)=\frac{1}{4}\left(\frac{K_I}{K_{II}}-\mathrm{sgn}(K_{II})\sqrt{\left(\frac{K_I}{K_{II}}\right)^2+8}\right),\quad -\pi<\theta<\pi \quad (8)$$

Where [sgn(K_{II})] represents the sign function. This function is commonly used in equations where the direction of fracture propagation or the sign of a quantity matters.

2.3. Mixed Mode of Cracks (I-II)

In the context of hydraulic fracturing, cracks in subsurface formations are rarely subjected to opening (Mode I) or shearing (Mode II) conditions alone; instead, they often experience mixed-mode loading (Mode I-II) due to varying crack orientations, in-situ stresses, and fluid pressure. The Stress Intensity Factor (SIF) is a fundamental parameter in fracture mechanics that characterizes the stress field intensity near the crack tip, governing crack initiation and propagation. For mixed Mode I-II cracks, the SIF is expressed as two components: K_I (Mode I) and K_{II} (Mode II). This section evaluates these factors for cracks simulated using the XFEM and validated against the BEM, focusing on their dependency on crack angle and interaction effects. The SIFs for a crack under mixed-mode loading can be derived from the stress field around the crack tip in a polar coordinate system (r, θ), where r is the radial distance from the tip and θ is the angular position. For an isotropic material, the near-tip stress field is approximated as [28]:

$$\sigma_{ij}=\frac{K_I}{\sqrt{2\pi r}}f_{ij}^{I}(\theta)+\frac{K_{II}}{\sqrt{2\pi r}}f_{ij}^{II}(\theta) \quad (9)$$

Where σ_{ij} is the stresses components ($\sigma_{xx}, \sigma_{yy}, \sigma_{xx}$), K_I is the mode I (SIF), reflecting tensile stress perpendicular to the crack plane; K_{II} is the mode II (SIF), reflecting shear stress parallel to the crack plane, and $f_{ij}^{I}(\theta), f_{ij}^{II}(\theta)$ Angular functions specific to each mode. For a crack of length $2a$ inclined at an angle β to the horizontal axis under far-field stresses σ (normal) and τ (shear), the SIFs are [28]:

$$K_I = \sigma\sqrt{\pi a}\sin^2\beta + \tau\sqrt{\pi a}\sin\beta\cos\beta \qquad (10)$$

$$K_{II} = \sigma\sqrt{\pi a}\sin\beta\cos\beta + \tau\sqrt{\pi a}\cos^2\beta \qquad (11)$$

These equations show that K_I and K_{II} vary with crack orientation (β), with K_I dominating at $\beta = 90^{o}$ (Mode I) and K_{II} peaking at intermediate angles ($\beta = 45^{o}$). In hydraulic fracturing, fluid pressure inside the crack adds an additional term, $p\sqrt{\pi a}$, to K_I, enhancing crack opening. In this study, XFEM is employed to compute K_I and K_{II} for three configurations: (1) single cracks at angles β=0°, 15°, 30°, 60°, (2) single cracks assessing crack opening displacement at 15° and 60°, and (3) multiple interacting cracks at 60° and 120°. XFEM's enrichment functions model the crack-tip singularity and discontinuity, allowing precise SIF extraction without re-meshing. The interaction integral method is typically used in XFEM to compute SIFs [28]:

$$I = \int_A \left[\sigma_{ij}\frac{\partial u_i^{aux}}{\partial x_1} - W\delta_{1j}\right]\frac{\partial q}{\partial x_j}dA \qquad (12)$$

Here u_i^{aux} is an auxiliary displacement field, W is the strain energy density, and q is a weighting function. This integral separate K_I and K_{II} contributions, validated against BEM's boundary-focused solutions.

2.4. Rock Fracture Toughness

Fracture toughness is a key mechanical property of rocks, indicating their resistance to fracture and crack propagation. Experimental fracture tests involve applying various stresses to rock samples to measure their fracture toughness. Computational methods use theoretical models and relationships to predict fracture toughness. Stress intensity factors are used to determine the maximum stress a material can withstand at the crack tip, beyond which the crack propagates rapidly. This critical stress intensity serves as a measure of fracture toughness, which is related to crack length and fracture toughness [29].

$$\sigma_f = \frac{K_{IC}}{\alpha\sqrt{\pi a}} \qquad (13)$$

Where α is a geometric parameter equal to 1 for edge cracks and generally has unit values for other positions. The α parameter has been tabulated for a wide range of samples and crack geometries, and special finite element methods are available for calculating it for new positions.

$$\sigma_f = \sqrt{\frac{EG_c}{\pi a}} \qquad (14)$$

$$K_I = -\int_{-a}^{a}\frac{1}{\sqrt{\pi a}}\sqrt{\frac{a-x}{a+x}}f(x)\,dx \qquad (15)$$

Stress intensity and energy considerations are related, as can be seen by comparing equations (14) and (15) with α=1.

$$\sigma_f = \sqrt{\frac{EG_c}{\pi a}} = \frac{K_{Ic}}{\sqrt{\pi a}} \rightarrow K_{Ic}^2 = EG_c \qquad (16)$$

This relationship holds in plane stress conditions and is slightly different in plane strain conditions.

$$K_{Ic}^2 = EG_c(1-\nu^2) \qquad (17)$$

For metals with $\nu = 0.3,\ (1-\nu^2) = 0.91$, this change is not significant. However, numerical values of or in plane stress or plane strain conditions are quite different. Typically, fracture toughness of rock is influenced by various factors such as chemical composition, internal structure, and environmental conditions (such as humidity and temperature) [24]. The fracture toughness values for different rocks are listed in Table 2 [30].

Table 2. Fracture toughness of different rocks [30].

Rock (Location/comment)	Fracture toughness (MPa√m)	Rock (Location/comment)	Fracture toughness (MPa√m)
Andesite (Tampomas)	1.26–1.68	Limestone (Bedford)	1.1
Basalt	1.73	Limestone (/white)	2.21
Basalt	3.01	Marble (/Fine grain)	0.96
Dolerite (Whin sill)	3.26	Marble (Ekeberg)	2.62
Gabbro (Kallax/series 1)	2.58	Sandstone	0.67

2.5. Role of Energy Balance in Crack Growth

The first systematic study of fracture phenomena was conducted by Griffith, who suggested that crack growth depends on the balance between strain energy and surface energy. He assumed that if the strain energy released during crack advancement exceeds the energy needed to create a new surface, unstable crack growth occurs [31].

$$G \geq 2\Gamma \tag{18}$$

The strain energy release rate (G) represents the energy released per unit area of crack growth and the work required to create a new crack surface. It depends on both the applied loading and crack size. Considering the elastic work needed to close the crack tip, Irwin established a relationship between G and the stress intensity factor, expressed as follows [31].

$$G\alpha = K^2 \tag{19}$$

The proportionality constant in the above equation is a function of the material's elastic constants. This relationship provides a connection between the stress field at the crack tip and the energy balance criterion for crack growth. It can now be interpreted in terms of the required (K) values for crack growth.

3. Governing Equations and Solution Procedures

The mathematical equations offer a brief overview of the governing equations for elastostatics and present their corresponding weak form. Specifically, it focuses on the case where an internal boundary exists, across which the displacement field may experience discontinuity.

The momentum equation in the context of fracture mechanics typically relates to the dynamic behavior of crack propagation. The equation can be written as [32]:

$$\rho \frac{\partial \mathbf{v}}{\partial t} + \nabla \cdot \sigma + \mathbf{f} = 0 \tag{20}$$

Where ρ is the density of the material, $\mathbf{v}$ is the velocity field, σ is the stress tensor, $\mathbf{f}$ is the body force vector (gravitational forces), and $\nabla \cdot \sigma$ is the divergence of the stress tensor, representing internal forces within the material. Consider a domain Ω bounded by the surface Γ. The boundary Γ is divided into subsets, Γ_t, and Γ_c, such that $\Gamma = \Gamma_u \bigcup \Gamma_t \bigcup \Gamma_c$, as illustrated in Figure 5. Prescribed displacements are applied on Γ_u, while tractions are specified on Γ_t. The crack surface Γ_c (represented as lines in 2D and surfaces in 3D) is assumed to be free of tractions [32]. The equilibrium equations describe the balance of internal stresses and external forces in a solid containing crack. The following equation governs this equilibrium [33]:

$$\nabla \cdot \sigma + F_b = 0 \qquad in\ \Omega \tag{21}$$

Where (σ) is the Cauchy stress tensor, (F_b) represents the body force vector, and (Ω) is the domain, including crack regions. This equation ensures that stress redistribution around cracks and the interaction of internal and external forces maintain equilibrium in the fractured medium. The boundary conditions define the interactions between the solid and its surroundings, including applied loads and crack surfaces. The following equations represent the boundary conditions for a cracked domain [34]:

$$\begin{aligned} \sigma \cdot \mathbf{n} &= F_{\bar{t}} \qquad \text{on } \Gamma_t \\ \sigma \cdot \mathbf{n} &= 0 \qquad \text{on } \Gamma_{c^+} \\ \sigma \cdot \mathbf{n} &= 0 \qquad \text{on } \Gamma_{c^-} \end{aligned} \tag{22}$$

Where Γ_t is traction boundary, Γ_u is displacement boundary, Γ_c is crack boundary, σ is Cauchy stress tensor, $\mathrm{F}_{\boldsymbol{b}}$ is body force vector, $\mathbf{n}$ is denoting the unit outward normal vector, and F_t is external traction vector [34].

$$\varepsilon = \varepsilon(\mathbf{u}) = \nabla_s \mathbf{u} \tag{23}$$

Here ∇_S denotes the symmetric part of gradient operator. The boundary conditions are as follows:

$$\mathbf{u} = \bar{\mathbf{u}} \quad \text{on} \quad \Gamma_u \tag{24}$$

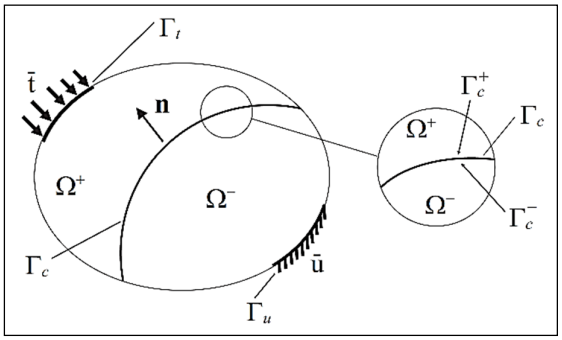

Figure 5. Body with internal boundary subjected to loads [34].

The constitutive relation is defined by Hooke's law, which relates stress and strain in linear elasticity [34].

$$\boldsymbol{\sigma} = \mathbf{C} : \varepsilon \tag{25}$$

Here $\boldsymbol{\sigma}$ is the Cauchy stress tensor, ε is the strain tensor, and **C** is the Hooke's constant (stiffness tensor), which representing the material's elastic properties. The symbol (**:**) denotes the double-dot product of tensors.

4. Numerical Solutions

The crack propagation mechanism due to hydraulic fracturing process can be numerically simulated using the extended finite element method (XFEM). The solution results can be verified by the analytical and semi-analytical solutions. In this research, the semi-analytical indirect boundary element method is used as a basis for verification of the simulated results.

4.1. Extended Finite Element Method

The Extended Finite Element Method (XFEM) is an advanced computational technique used to model and simulate crack propagation and other discontinuities in materials. It extends the traditional Finite Element Method (FEM) by enriching the solution space with additional functions that can represent discontinuities, such as cracks, within elements without needing to re-mesh as cracks grow. XFEM is particularly effective in modeling problems involving fracture mechanics, including crack initiation, propagation, and complex crack behavior in materials subjected to mechanical loading. It is widely used in engineering fields to analyze structures where cracks or other discontinuities may develop and evolve over time.

In the presence of a crack, the solution space must accommodate functions that can represent discontinuities in the displacement field. Therefore, the weak form of the equilibrium equation in XFEM is expressed as [29, 30]:

$$\int_\Omega \sigma : \nabla v \, d\Omega - \int_\Omega b \cdot v \, d\Omega - \int_{\Gamma_t} t \cdot v \, d\Gamma - \int_{\Gamma_T} [\![t]\!] \cdot v \, d\Gamma = 0 \tag{26}$$

Where Ω is the domain of the body under study, Γ is the boundary of the domain Ω, Γ_T is the fracture surface, σ is the stress tensor, b is the body force, t is the boundary traction, $[\![t]\!]$ denotes the jump in traction across the crack, and v is the test function or weight function. For a single crack in two dimensions, let (Γ_c) represent the crack surface (interior) and (Λ_c) denote the crack tip, with the closure ($\bar{\Gamma}_c = \Gamma_c \cup \Lambda_c$). Now, consider a point ($\mathbf{x}$) located within a finite element (e). The enriched displacement approximation for a vector-valued function ($\mathbf{u}^h(\mathbf{x}) : \square^2 \to \square^2$) is expressed as [36]:

$$\mathbf{u}^h(\mathbf{x}) = \sum_{I \in \square} N_I(\mathbf{x}) \mathbf{u}_I + \sum_{I \in \square_\Gamma} N_I(\mathbf{x}) H(\mathbf{x}) \mathbf{a}_I + \sum_{I \in \square_\Lambda} N_I(\mathbf{x}) \left[\sum_{\alpha=1}^{4} F_\alpha(\mathbf{x}) \mathbf{b}_I^\alpha \right] \tag{27}$$

In this formulation, (N_I) represents the standard finite element shape function corresponding to node (I), while ($\mathbf{u}_I$) denotes the nodal displacement vector associated with the continuous part of the finite element solution. The term ($\mathbf{a}_I$) is the nodal enriched degree of freedom vector linked to the Heaviside (discontinuous) function, and ($\mathbf{b}_I^\alpha$) is the nodal enriched degree of freedom vector associated with the asymptotic crack-tip function. In the equation, ($\square = \{n_1, n_2, ..., n_m\}$) refers to the set of all nodes within an element [36].

$$\square_\Lambda = \{ n_K : n_K \in \square, \ \bar{\omega}_K \cap \Lambda_c \neq \emptyset \} \tag{28}$$

$$\square_{\Gamma}=\{n_J : n_J \in \square,\ \omega_J \cap \Gamma_c \neq \emptyset\ ,n_J \notin \square_{\Lambda}\} \quad (29)$$

$$\square_{\Lambda} \cap \square_{\Gamma} \neq \emptyset \quad (30)$$

Here ($\square_{\Gamma}$) represents the nodes whose shape function support is intersected by the crack interior (Γ_c), and ($\square_{\Lambda}$) denotes the nodes whose shape function support is intersected by the crack tip (Λ_c), $\bar{\omega}=\text{supp}(n_K)$ is the support of the nodal shaped function, which consists of the union of all crack-tip elements with n_K as one of its vertices. Similarly, $\omega=\text{supp}(n_J)$ is the support of the nodal shaped function, which consists of the union of all crack interior elements with n_J as one of its vertices. The definition of the enrichment support domain is illustrated in Figure 6. The circled nodes are enriched by the crack-tip function F_α whereas squared nodes are enriched by the jump function *H*.

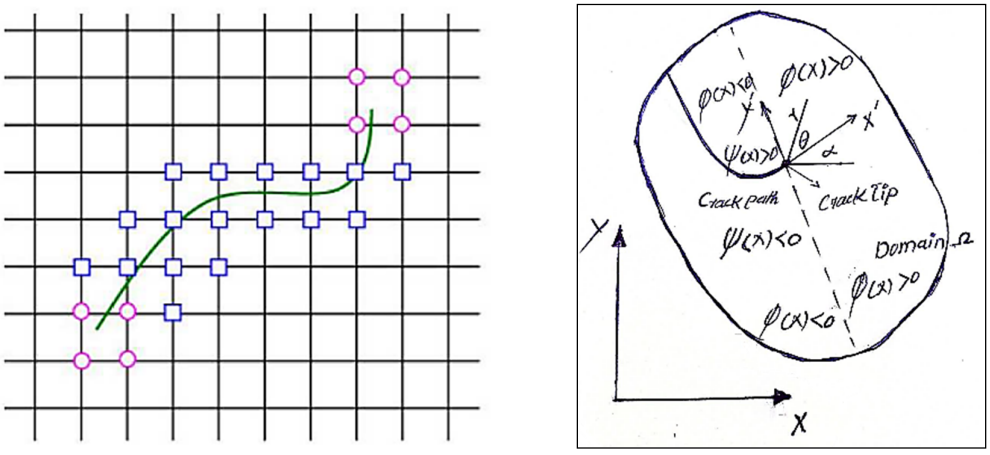

(a) (b)

Figure 6. (a): The set of nodes elected for enrichment, (b): Polar coordinates at crack tip [36].

For crack problem, two sets of enrichment function are used:

- The function $H(\mathbf{x})$, the modified Heaviside function which takes on the value (+1) above the crack and (−1) below the crack.
- The function $F_\alpha(\mathbf{x})$, which is a basis that spans the crack-tip asymptotic fields [36].

$$F_\alpha(r(\mathbf{x}),\theta(\mathbf{x}))=\left\{\sqrt{r}\sin\frac{\theta}{2},\ \sqrt{r}\cos\frac{\theta}{2},\ \sqrt{r}\sin\frac{\theta}{2}\sin\theta,\ \sqrt{r}\cos\frac{\theta}{2}\sin\theta\right\} \quad (31)$$

Where (r,θ) is a polar co-ordinate system with its origin at the crack-tip and $\theta=0$ tangent to the crack at its tip, as show in Figure 6. Note that ($\sqrt{r}\sin(\theta/2)$) takes into account the discontinuity across the crack face. The Extended Finite Element Method (XFEM) in Abaqus enables efficient crack modeling without requiring the mesh to align with crack geometry. It enhances fracture simulation through crack-tip enrichment, which introduces additional degrees of freedom (DOFs) to capture stress singularities, and the phantom node method (PNM), which allows progressive crack opening by duplicating and separating nodes based on the cohesive traction-separation law. Abaqus employs the Heaviside function for fully cut elements and an asymptotic function for crack-tip regions, with the level set method dynamically updating crack geometry [37] . By combining crack-tip enrichment and phantom nodes, XFEM in Abaqus accurately models stress fields and seamless crack propagation while maintaining numerical stability. These techniques improve fracture modeling efficiency, making XFEM a powerful tool for simulating complex crack behavior in engineering applications [38].

4.2. Boundary Element Method

The boundary element method is among the most effective numerical techniques for solving problems in fracture mechanics. In boundary value problems, an integral equation defined within a specific domain can be transformed into a boundary integral equation over the boundary of that domain. To numerically solve the boundary integral equation, the domain's boundary must be divided into segments, referred to as boundary elements. The BEM is based on Betti's reciprocal theorem. Assuming that (1) represents the loading of interest and (2) represents a reference loading with a known solution, Betti's theorem, in the absence of body forces, can be expressed as follows [39].

$$\int_S T_i^{(1)} u_i^{(2)} dS = \int_S T_i^{(2)} u_i^{(1)} dS \quad (32)$$

Here (S) represents the boundary of the domain, (T_i) and (u_i) are the components of the traction and displacement vectors, respectively, and the superscripts indicate the loading cases (1) and (2). By applying Betti's reciprocal theorem to the boundary conditions, when a unit force is applied at an interior point ($\mathbf{X}'$), it generates displacements and tractions at the surface point (x), resulting in [39]:

$$u_i(\mathbf{X}') = -\int_S T_{ij}(\mathbf{X}', \mathbf{x}) u_j(\mathbf{x}) dS(\mathbf{x}) + \int_S U_{ij}(\mathbf{X}', \mathbf{x}) t_j(\mathbf{x}) dS(\mathbf{x}) \quad (33)$$

Here T_{ij} and U_{ij} represent the fundamental solutions, $u_i(\mathbf{X}')$ denotes the displacement vector at the interior point $\mathbf{X}'$, and $u_j(\mathbf{x})$, and $t_j(\mathbf{x})$ are the reference displacement and traction vectors at the boundary point $\mathbf{x}$. If $\mathbf{X}'$ approaches $\mathbf{x}$, where, $\mathbf{x}$ is a boundary point, equation (33) transforms into:

$$\frac{1}{2} u_i(\mathbf{x}') + \int_S T_{ij}(\mathbf{x}', \mathbf{x}) u_j(\mathbf{x}) dS(\mathbf{x}) = \int_S U_{ij}(\mathbf{x}', \mathbf{x}) t_j(\mathbf{x}) dS(\mathbf{x}) \quad (34)$$

Assuming the boundary is smooth, solving for the unknown boundary data requires dividing the boundary into elements and approximating the equation with a system of algebraic equations.

The BEM is a powerful alternative to the FEM, offering the key advantage of reducing the problem's dimensionality by one. This results in a smaller system of equations and less data for analysis. BEM is particularly beneficial for problems with frequent modifications, as it simplifies mesh generation and eliminates the need for complete re-meshing, making it more compatible with existing solid modelers and mesh generators [39].

5. Numerical Modeling Procedures

In numerical modeling of fracture mechanics, ensuring accuracy and reliability requires a structured approach. This section covers the key procedures, including initialization, mesh sensitivity analysis, and verification. Proper initialization defines the problem setup, mesh sensitivity examines the influence of discretization, and verification ensures the correctness of the numerical implementation.

5.1. Initialization of Numerical Modeling

The first step of modeling involves identifying and establishing an initial analytical solution and numerical modeling to compute and determine the crack aperture, ensuring the accuracy and validity of the modeling approach. In this phase, an analytical method is employed to evaluate the crack aperture, which serves as a benchmark for validating the chosen numerical method. This process is initially formulated while considering the appropriate boundary conditions. The initial geometric model consists of a planar crack embedded in an infinite domain under internal pressure. To validate the developed code, the problem is formulated based on the *Constant Element Poroelastic Displacement Discontinuity Method* (CEP-DDM). In this model, an extremely thin crack with (2L) length; is considered within an elastic medium subjected to a constant internal pressure. Additionally, the relative normal displacement of the crack surfaces (crack opening w_f), is derived analytically by the following equation [40].

$$w_f = \frac{2p(1-v)}{G} \sqrt{L^2 - x^2} \quad (35)$$

Where (x) in $-L \le x \le L$ is interval and G is the shear modulus. The elastic modulus, E is determined using the following equation.

$$E = 2G(1+v) \quad (36)$$

Where v is Poisson's ratio. The input material parameters are taken from an analytical solution method which presented in the Table 3. The problem has been analyzed using the proposed numerical method. At the moment of loading, the medium responds elastically (undrained condition), and the model's response corresponds

to that of an elastic system with appropriate undrained coefficients [40].

Table 3. Input parameters for model verification of a pressurized crack problem in an elastic media [40]

Input Parameters	
E (GPa)	34.06
v	0.31
P_{inj} (MPa)	30
G (MPa)	13
2L (m)	1
X	From -0.5 to +0.5

The elastic modulus, shear modulus, and Poisson's ratio significantly influence the model response. A sensitivity analysis can determine how variations in these parameters affect crack aperture and stress distribution around the crack tip. This aspect will be further examined to ensure the robustness of the numerical model. Additionally, in the discussion and conclusion section, the analysis sensitivity is presented in more detail to highlight the effect of these parameter variations on fracture behavior. For an appropriate simulation and verification using the XFEM, the geometry of the model is assumed to be finite, and tensile stress is applied along the Y-axis at the upper and lower boundaries of the model in opposite directions. Additionally, the boundary conditions along the X-axis are fixed, meaning there is no horizontal displacement at the vertical boundaries of the model. These boundary conditions ensure a realistic simulation of crack initiation and propagation while preventing rigid body motion. Proper constraints along the X-axis and applied tensile stress along the Y-axis help achieve accurate fracture modeling using XFEM. In Figure 7 (a) shows the boundary conditions and the applied force method; and (b) shows the meshing form around the initial crack.

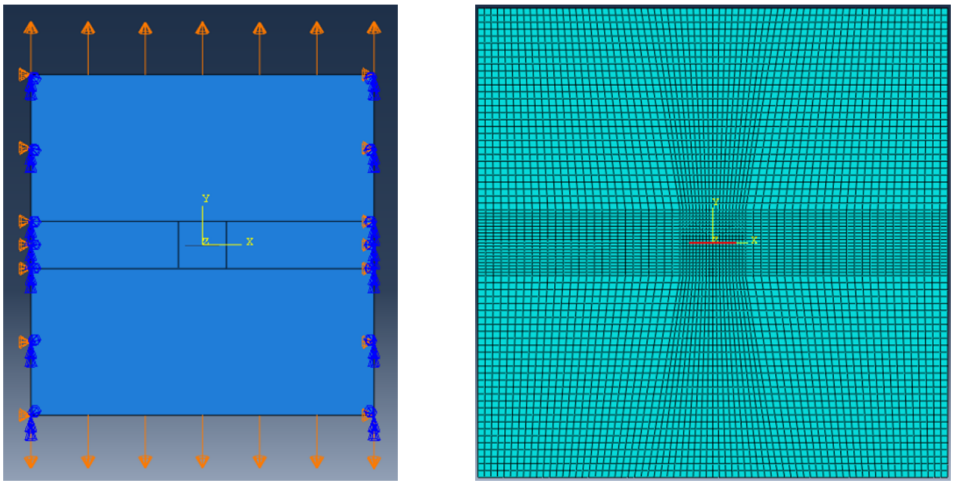

(a) **(b)**

Figure 7. (a): Boundary conditions and applied force method, (b): meshing form around the initial crack.

The degeneration of elements and the collapse of nodes near the crack tip leads to a more intricate mesh geometry, as depicted in Figure 7-b. The model consists of the CPS4R element type, a quadrilateral element shape, a linear geometric order, and a total of 5767 nodes and 5616 elements (Figure 8). In this modeling, these types of elements and nodes are used to accurately capture the mechanical behavior of the structure under the given conditions. It is widely applied in mechanical problems, particularly in stress and strain analysis of elastic materials. Each node has two degrees of freedom (displacement in the (x) and (y) directions), allowing for accurate modeling of structural deformations. To ensure precise results, the mesh must be carefully designed, especially near the crack tip, where quadrilateral elements collapse into triangular shapes to capture the stress singularity effectively. This refinement is crucial for modeling high-stress gradients and deformation patterns, improving numerical accuracy, enhancing convergence, and minimizing errors, as supported by Dassault Systems [41].

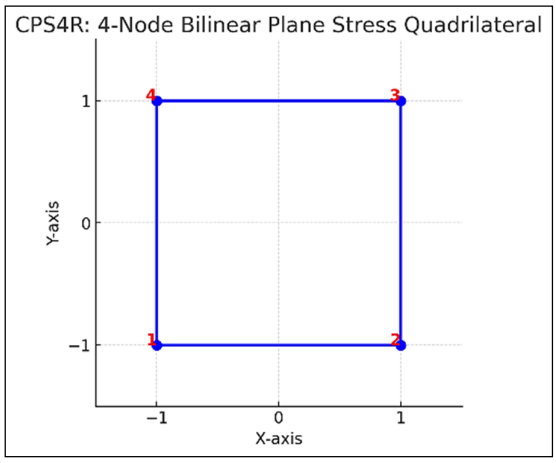

Figure 8. CPS4R element 4 node bilinear quadrilateral for plane stress analysis.

Here is a visual representation of the CPS4R (4-node bilinear plane stress quadrilateral) element. The red numbers indicate the node numbering in counterclockwise order.

5.2. Mesh Sensitivity and Related Explanations

In Finite Element Analysis (FEA), mesh sensitivity refers to how dependent the simulation results (such as stress, strain, or displacement) are on the size and type of elements used in the mesh. One critical aspect in this regard is the selection of an appropriate element type, here specified as CPS4R. The CPS4R element is a quadrilateral element with four nodes, where "C" stands for continuum, "P" for Plane, "S" for Stress (indicating plane stress conditions), "4" denotes the number of nodes, and "R" stands for Reduced Integration. This element is commonly used in two-dimensional problems under plane stress conditions. The reason for choosing CPS4R is that it provides a good balance between accuracy and computational efficiency. The reduced integration technique helps prevent shear locking in problems involving large deformations and reduces computation time. However, care must be taken to avoid issues like "hourglassing," which may require additional scrutiny. The XFEM is designed to model discontinuities, such as cracks, without requiring the mesh to confirm to the discontinuity geometry. To ensure convergence in XFEM, several key factors must be considered. The mesh size must be sufficiently refined, particularly near discontinuous regions like crack tips, to accurately capture sharp field variations, such as stress singularities. XFEM employs enrichment functions to describe the behavior of discontinuities, and selecting appropriate functions, such as singular functions for crack tips, is critical for convergence. To confirm convergence, analyses are typically conducted with progressively finer meshes, and results, such as stress intensity factors, are compared; convergence is achieved when further mesh refinement produces negligible changes in the results [42].

5.3. XFEM Modeling and Verification for Pressurized Crack Problem

The second step of modeling focuses on model verification, which involves systematically comparing simulation outcomes with established theoretical or experimental benchmarks. This process ensures the model's ability to replicate real-world fracture mechanics phenomena, such as crack initiation, propagation, and stress distribution under predefined loading and boundary conditions. To validate accuracy, critical quantitative metrics including SIFs, fracture propagation paths, and energy release rates are analyzed and matched against reference data. This rigorous verification step confirms the model's fidelity in capturing the underlying physics of fracture behavior and guarantees its reliability for further predictive analysis. The SIF for an infinite plate containing a central crack under tensile loading, based on LEFMs is calculated using the following Equation [43].

$$K_I \approx \sigma \sqrt{\pi L}\left(1-\frac{L}{2b}\right)\left(1-\frac{L}{b}\right)^{-1/2} \quad (37)$$

The critical SIF is derived from following Equation as outlined in this section [43].

$$K_{Ic} \approx \frac{F_c}{2b}\sqrt{\pi L}\left(1-\frac{L}{2b}\right)\left(1-\frac{L}{b}\right)^{-1/2} \quad (38)$$

While, the critical fracture energy is determined via Equation (14) [43].

$$G_e = \frac{1-\nu^2}{E}K_I^2 \quad (39)$$

In the XFEM simulation of fracture propagation, the critical load required to initiate crack growth is identified as 30 GPa (Figure 9). This figure illustrates the STATUSXFEM parameter, a numerical output indicating the progression of the fracture. Non-zero values of STATUSXFEM represent active crack propagation, whereas a value of 1 denotes the complete degradation of cohesive interactions within the fractured section [44].

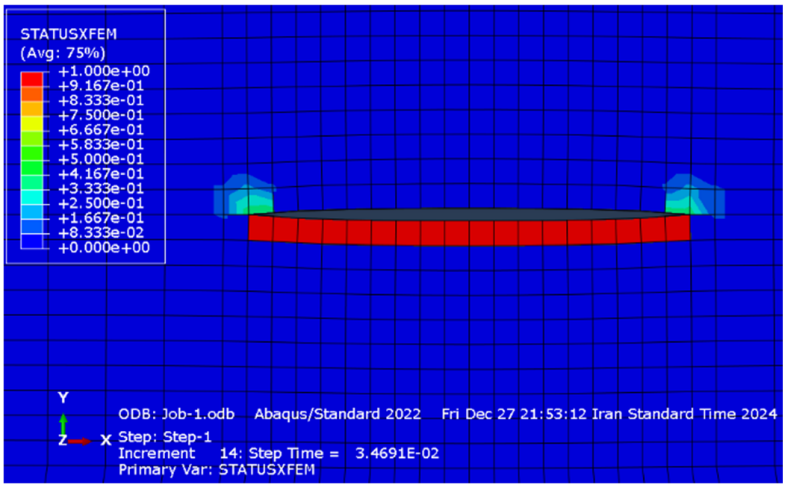

Figure 9. Status for crack initiation and growth using XFEM.

For an accurate simulation and validation using the XFEM, the model's geometry is considered finite, and tensile stress is applied in opposite directions along the Y-axis at the upper and lower boundaries. The crack opening displacement and fracture behavior are analyzed using equations (35) and (36), which provide a mathematical framework for evaluating crack initiation and growth under tensile loading. These equations play a crucial role in predicting the fracture response of the material and ensuring the reliability of the numerical simulation.

The COD is calculated within the interval [-0.5, 0.5] with a step size of 0.5. This structured interval allows for a systematic evaluation of displacement variations along the crack front under applied loading conditions. To analyze the crack growth behavior, the COD variations are simulated using the XFEM. This method effectively models crack formation and growth without requiring predefined crack paths, providing a more accurate representation of fracture mechanics. The computed COD values at each point in BEM example within the defined interval are presented in the Table 4, providing a clear numerical representation of displacement variations [40].

Table 4. Computed COD values at each point within the defined interval

x (m)	W_f (m)	x (m)	W_f (m)
0	0.00318	0	0.00318
0.1	0.00317	-0.1	0.00317
0.2	0.00312	-0.2	0.00312
0.3	0.00304	-0.3	0.00304
0.4	0.00292	-0.4	0.00292
0.5	0.00276	-0.5	0.00276
0.6	0.00255	-0.6	0.00255

The results from the XFEM simulation are then plotted to illustrate the displacement trends along the crack front. For validation, the obtained numerical results are compared with the analytical solution and BEM. Additionally, a comparative plot of the COD curve is generated to visually assess the consistency between the XFEM, BEM and the analytical solutions, ensuring the accuracy and reliability of the numerical model Figure 10.

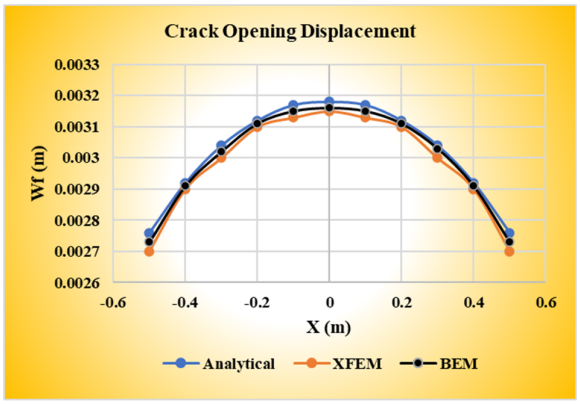

Figure 10. Comparing the XFEM, analytical and BEM results for COD values of the pressurized crack problem.

5.4. Numerical Error Analysis Between XFEM and BEM Results

To assess the accuracy of XFEM in modeling crack propagation, it is essential to validate its results against a benchmark solution such as the BEM. BEM is widely used for fracture mechanics problems due to its ability to provide highly accurate stress intensity factors (SIFs) with minimal meshing requirements. A comparative analysis between XFEM and BEM can highlight

numerical discrepancies and provide insights into error sources [45].

The numerical error between XFEM and BEM results can be analyzed using the relative error in stress intensity factors (SIFs) [32]:

$$E_{SIF} = \frac{|K_{XFEM} - K_{BEM}|}{K_{BEM}} \times 100\% \quad (40)$$

Here K_{XFEM} and K_{BEM} are the stress intensity factors computed using XFEM and BEM, respectively. A lower E_{SIF} value indicates a higher agreement between the methods [32].

XFEM requires adequate mesh refinement near the crack tip to capture the singular stress field. Coarser meshes can introduce errors in SIF estimation, leading to deviations from the BEM reference values. The choice of enrichment functions in XFEM affects its ability to approximate the exact solution. Improper selection of the enrichment zone may lead to localized errors, especially in complex crack paths. While BEM provides highly accurate results, its accuracy depends on the boundary discretization and kernel function approximations. Small numerical errors in BEM can propagate when used as a reference for validation. XFEM inherently supports complex crack paths, whereas traditional BEM formulations often rely on simpler geometries. This difference may cause slight variations in crack propagation predictions [45]. Comparing XFEM and BEM results provides a robust framework for validating crack propagation simulations. By analyzing SIF errors, adjusting mesh density, and refining enrichment strategies, the accuracy of XFEM can be improved. The validation process ensures that XFEM solutions remain reliable for practical fracture mechanics applications.

6. Results and Discussion

Numerical modeling serves as a cornerstone in fracture mechanics, offering a robust framework for analyzing crack behavior with high precision. In this study, the XFEM was employed to simulate crack formation, aperture opening, and propagation in hydraulic fracturing processes. To validate the computational model, a confined square domain was constructed, featuring a central crack and central cylindrical wellbore representing the fluid injection zone.

The investigation explored multiple crack configurations to assess their mechanical response:

- Single crack: A single crack oriented at specific angles relative to both axes (U1, U2).
- Effect of crack angle orientation on crack formation and growth state (XFEM).
- Multiple crack: A complex arrangement involving three or more interacting cracks.
- Analysis sensitivity of the model.Single Crack: A single crack oriented at specific angles relative to both axes (U1, U2)

This scenario examines the behavior of a single crack oriented at 0^o, 15^o, 30^o, and 60^o relative to the horizontal axis, focusing on crack formation and the corresponding crack opening displacement in the U1 (horizontal) and U2 (vertical) directions. A homogeneous geometry model without a central hole is used to analyze how varying crack orientations affect the initiation and propagation of cracks, with the results compared to those from a reference model to validate the methodology. Numerical and analytical techniques are employed to capture deformation patterns near the crack, revealing that lower angles (closer to 0^o) predominantly induce horizontal displacement while higher angles progressively increase the vertical component of displacement.

For a 0^o crack angle, the crack is aligned parallel to the horizontal axis (U1). Applying a tensile force along the y-axis primarily induces crack opening in the (U2) direction (vertical displacement), characteristic of mode I fracture. The crack opening displacement (COD) is symmetric about the horizontal axis, with tensile stresses concentrated along the crack faces. Horizontal displacement (U1) remains minimal and does not significantly contribute to crack propagation. Figure 11 illustrates the crack path (a) and its opening mode (b) at a zero-degree angle in (U1 and U2) directions.

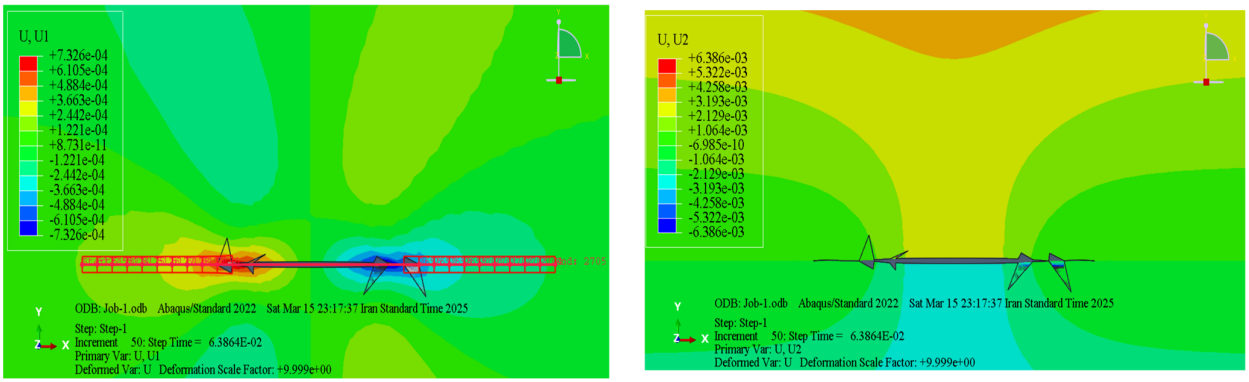

(a) **(b)**

Figure 11. Crack propagation path (a) and crack opening displacement at a 0° crack angle (b).

The analysis further indicates that deformation is primarily governed by vertical displacement (U2), while (U1) displacements remain negligible. This behavior aligns with linear elastic fracture mechanics expectations for mode I loading. The Figure 12 present displacement analysis in both (U1) and (U2) directions, demonstrating the extent of displacement in each direction and their influence on crack opening.

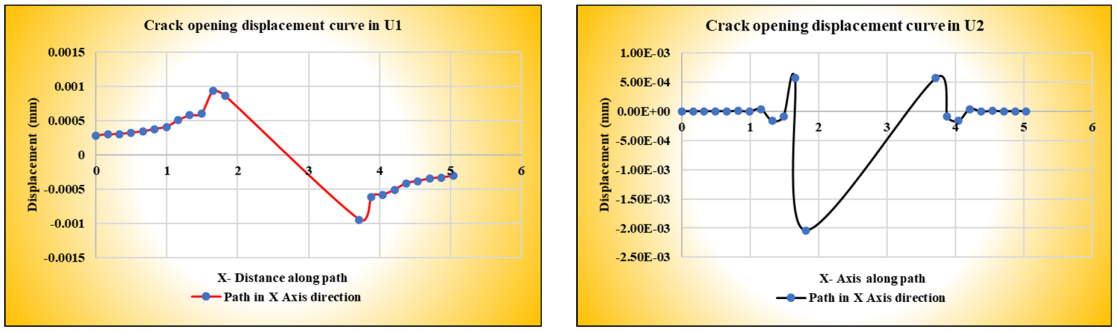

(a) **(b)**

Figure 12. Displacement analysis curve in both directions (U1, U2).

When a crack is inclined at 15° relative to the horizontal axis, shear components are introduced alongside tensile stresses. This configuration results in mixed-mode fracture behavior, where both horizontal (U1) (a) and vertical (U2) (b) displacements contribute to the overall crack opening. The path in both the x and y axes for analyzing crack formation and growth in the (U2) direction, which indicates the opening of the crack, is illustrated in the Figure 13. The stress intensity factors exhibit moderate mode II contributions due to the slight angular deviation from the horizontal, leading to a symmetry in the crack opening profile.

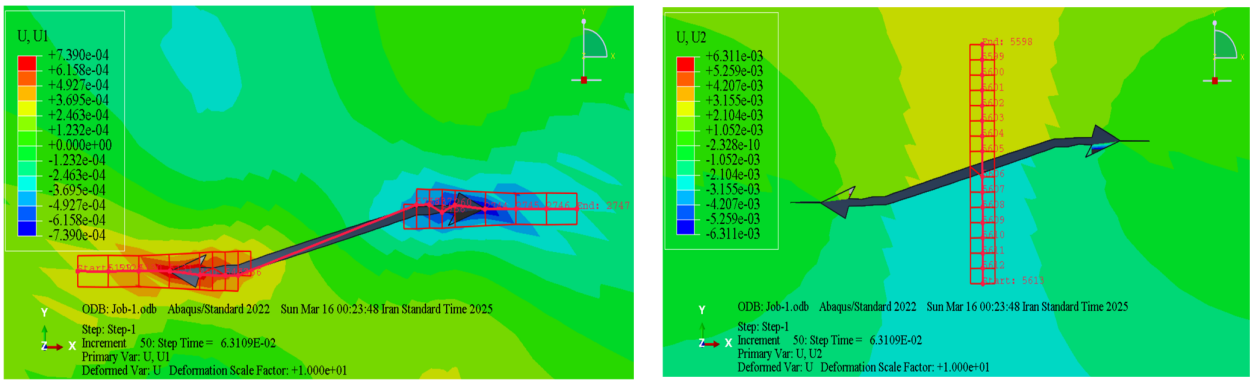

(a) **(b)**

Figure 13. Crack propagation path and COD in both axes (x, y) at a 15° crack angle.

The analysis shows that while the horizontal displacement remains dominant, the vertical component is no longer negligible, and the interaction between the two directions begins to influence the crack propagation path. Figures (a) and (b) show the crack opening displacement in U2 direction; that the analysis path is in the x and y axes direction. Also, the figures (c) and (d) shows the crack opening displacement curves in U1 direction which the analysis path are in x and y axes directions (Figure 14).

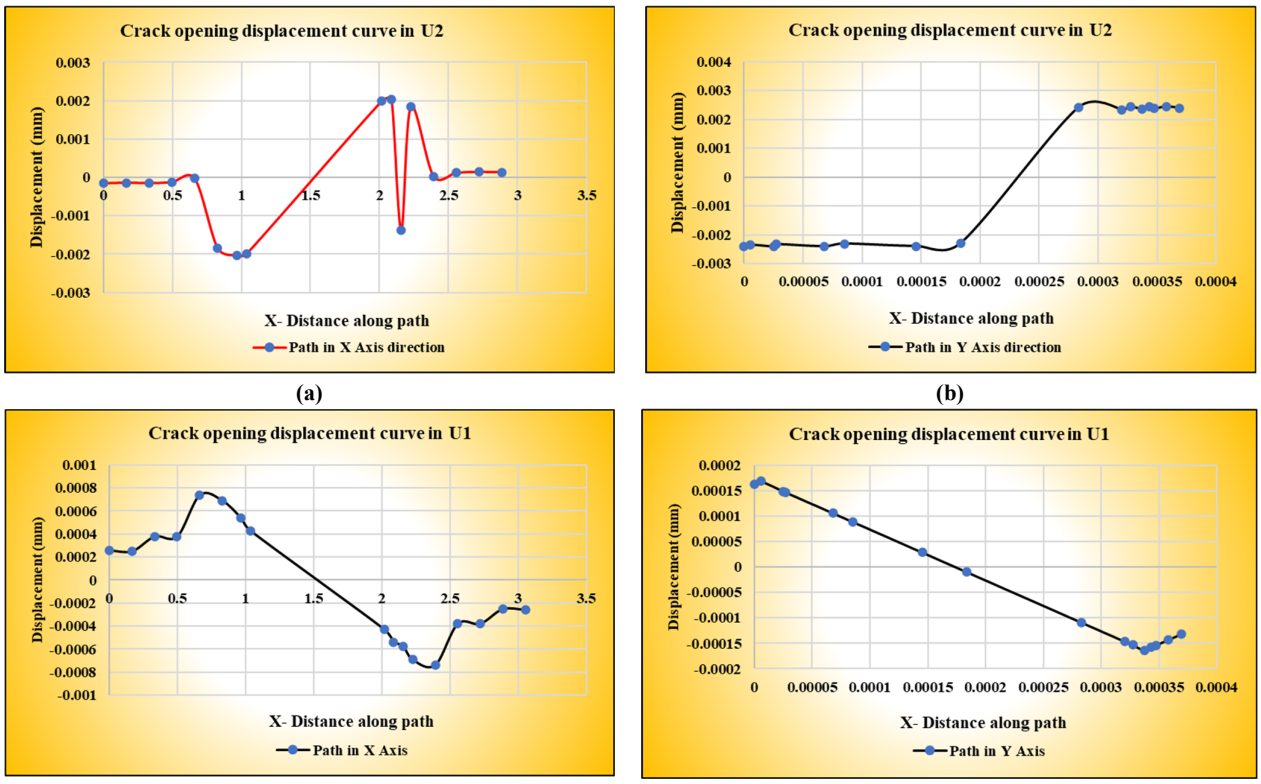

Figure 14. Crack opening displacement curves in (U1, U2) along x and y axes directions.

To analysis this behavior, numerical methods such as the (XFEM) can be employed to simulate the stress and displacement fields around the crack tip. This approach allows for a detailed understanding of the mixed-mode loading conditions and their effects on crack growth. Experimental studies can also provide valuable insights into the crack propagation under mixed-mode loading. By combining numerical simulations with experimental data, a comprehensive understanding of crack behavior under mixed-mode loading can be achieved, facilitating the development of more accurate predictive models for material failure.

For a 30^{o} crack orientation: At a 30^{o} orientation, the crack experiences a significant mix of both mode (I and II) loading, resulting in a pronounced coupling between horizontal and vertical displacements. Figure 15 (a and b), illustrates the crack opening mode at a 30^{o} angle.

The opening displacement is more balanced between U1 and U2, reflecting the increased influence of shear stresses on the crack faces. This mixed-mode behavior causes a more complex stress field near the crack tip, which can alter the crack propagation direction and increase the likelihood of crack branching or kinking. The detailed analysis demonstrates that the relative contributions of the U1 and U2 displacement components are nearly comparable, making this orientation particularly sensitive to variations in the applied load and material properties. Figure 16 (a and b), shows the COD curves in both directions (U1, U2).

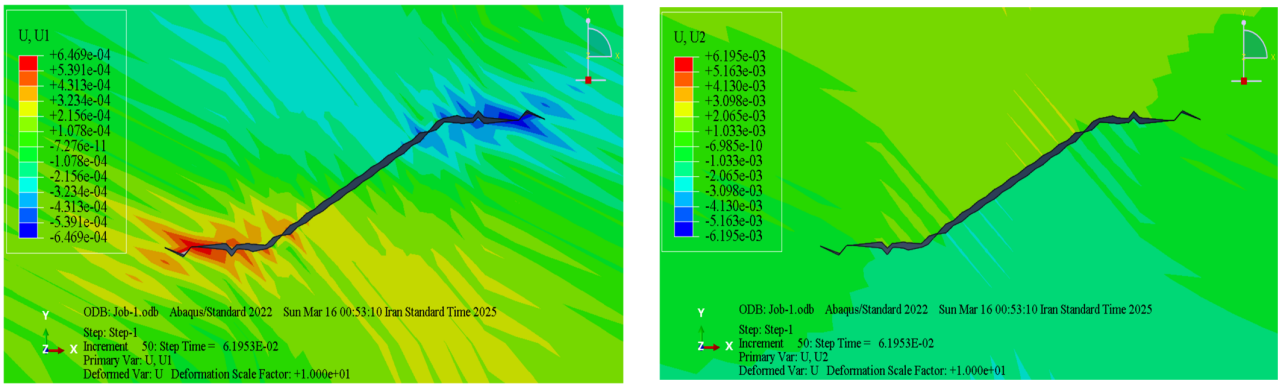

(a) **(b)**

Figure 15. Crack opening displacement at 30° in (U1, U2) directions.

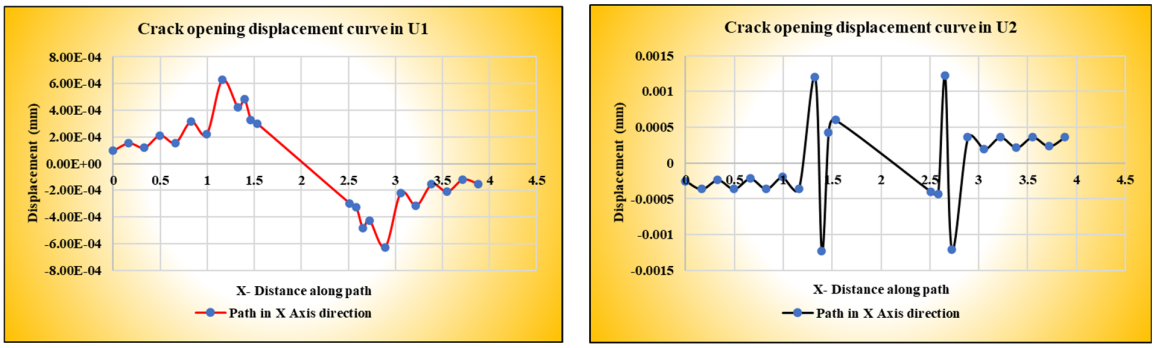

(a) **(b)**

Figure 16. The crack opening displacement curves in the U1 and U2 directions.

For a 60° crack orientation: When the crack is oriented at 60° with respect to the horizontal axis, the vertical (U2) displacement becomes the predominant mode of crack opening. The following figures (a and b) illustrate the crack opening displacement at 60° in both direction (U1, U2) Figure 17.

In this section the crack is nearly aligned with the vertical direction, so the tensile stress induces a significant opening in the U2 direction, while the horizontal displacement (U1) plays a secondary role. The stress intensity factor is largely governed by mode I loading in the vertical direction, although residual shear effects are still present due to the angular orientation. The analysis reveals that the crack propagation is strongly directed along the path of maximum tensile stress in the vertical axis, leading to a more pronounced asymmetry in the crack opening profile compared to lower angles, and potentially influencing the subsequent fracture process in a manner that favors vertical propagation. Figure 18 (a and b), shows the crack opening displacement curves in the U1 and U2 directions.

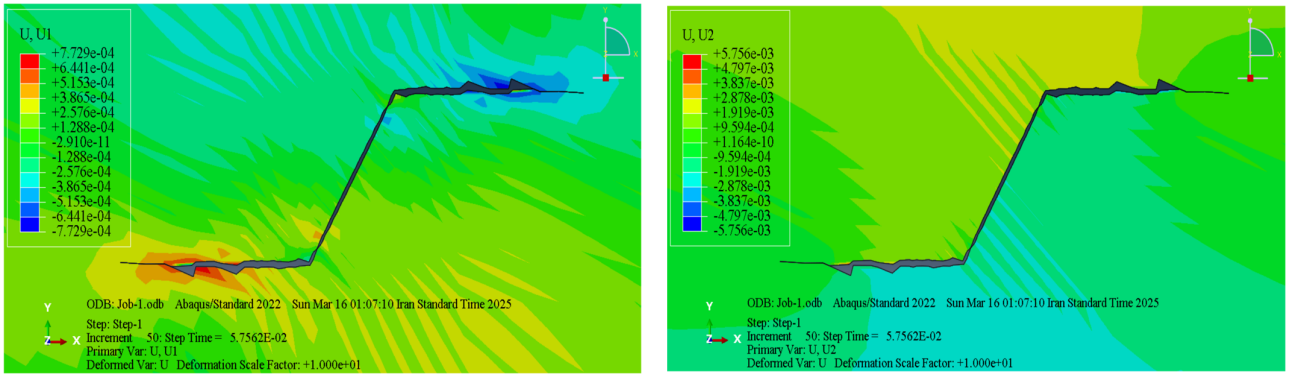

(a) **(b)**

Figure 17. Crack opening displacement along U1 and U2 directions at 60°.

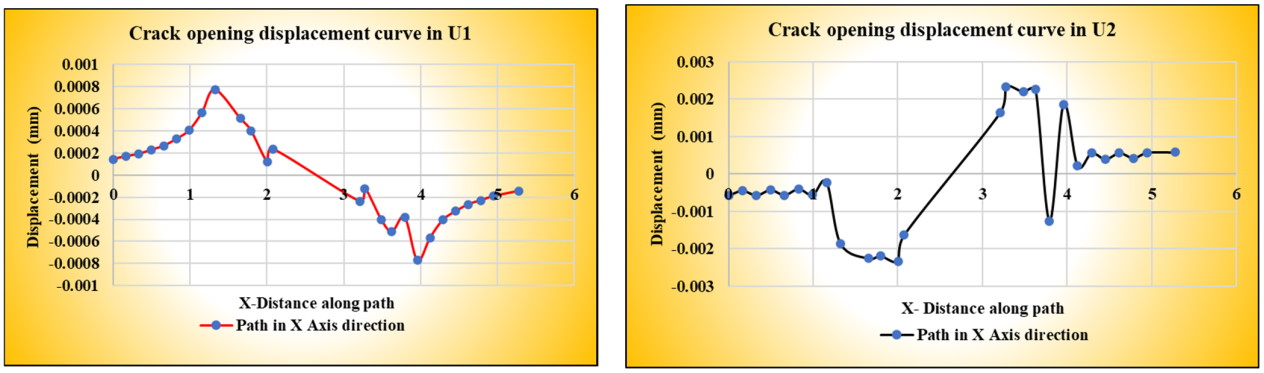

(a) (b)

Figure 18. Crack opening displacement curves in the U1 and U2 directions.

As the crack angle increases from 0° to 60°, the maximum displacement occurs in the U2 direction, and the highest crack opening displacement is observed at 60°. These changes indicate the influence of crack orientation on stress distribution and localized deformation. Numerical analysis also reveals that with increasing crack angle, the crack growth path alters, and stress concentration at the crack tip intensifies, potentially leading to early instability and accelerated structural failure.

The crack angle, ranging from 0° (horizontal under vertical tensile loading) to 60° (inclined), critically affects crack growth and material failure, as explained by Linear Elastic Fracture Mechanics (LEFM). As the angle increases, the SIF shifts K_I (opening mode) decreases while K_{II} (shear mode) rises prompting greater crack deviation, consistent with the maximum circumferential stress criterion predicting growth toward maximum tensile stress. Numerical methods like XFEM and BEM confirm this trend, showing reduced K_I and increased K_{II} with rising angles, impacting crack stability and strain energy release rate (G), especially in brittle materials. Linking these findings to fracture mechanics theory validates numerical models and enhances understanding of crack propagation mechanisms.

6.1. Effect of Crack Angle Orientation on Crack Formation and Growth State (XFEM) (0° and 60°)

For the first orientation angle from 0° to 60°, to evaluate the effect of crack orientation angles on the formation and propagation state of cracks in XFEM, an angle of 15° has been selected for this scenario. Additionally, crack formation and growth up to 60° remain stable and can form and propagate normally. However, beyond this angle up to 90°, both crack formation and growth decrease. At a low angle (15°), the crack propagation follows a relatively stable and linear path, aligned closely with the initial crack orientation. Adhesion between crack surfaces plays a significant role in resisting crack opening, which reduces the likelihood of rapid crack growth. The fracture energy (G_c) required to propagate the crack is comparatively low, and the cohesive zone model would show gradual debonding, indicative of stable growth. The status of crack growth (a) and displacement curve (b) shown in Figure 19.

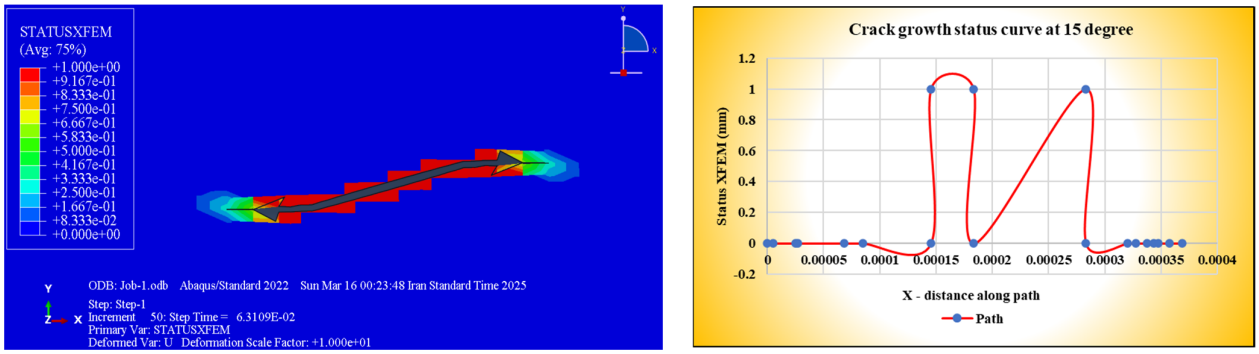

(a) (b)

Figure 19. Status of crack growth and displacement curve at 15°.

In this scenario, the stress intensity factor (SIF) for Mode I (K_I) is dominant, as tensile stresses primarily act to open the crack. The contribution of Mode II, SIF (K_{II}) is minor, due to the near-parallel alignment of the crack with the principal stress direction. The combined SIF ($K_{eff}=\sqrt{K_I^2+K_{II}^2}$) remains moderate, resulting in slower crack growth. The material's toughness (G_c) is not fully utilized, as the energy release rate (G) status below the critical value, ensuring a stable crack propagation process.

At 60°, the crack propagation becomes highly unstable, with a significant deviation in its path. This behavior is influenced by the increased normal stress acting perpendicular to the crack plane, which reduces the effectiveness of adhesion and facilitates rapid debonding. The fracture energy (G_c) is reached and exceeded quickly, leading to an unstable propagation process. The status of crack growth (a) and displacement curve at 60° has shown in Figure 20.

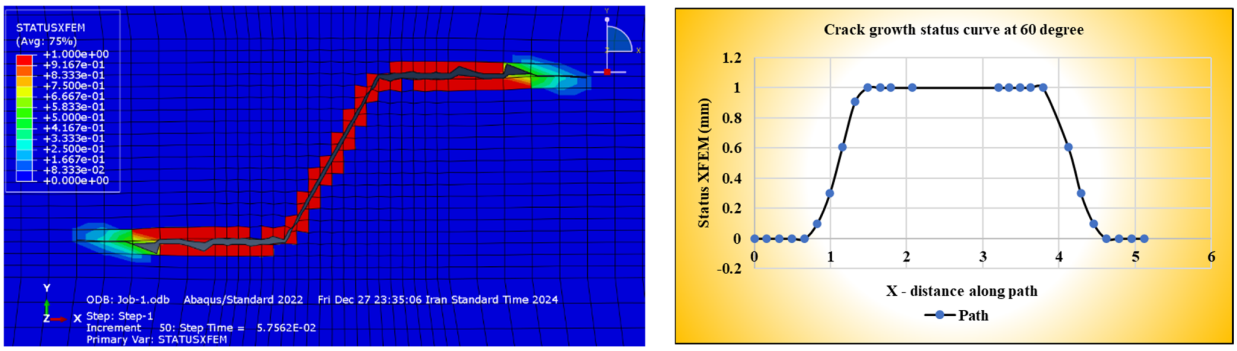

(a) (b)

Figure 20. Status of crack growth and displacement curve at 60°.

In this case, both Mode I (K_I) and Mode II (K_{II}) SIFs contribute significantly to the crack growth, creating a mixed-mode stress state. The effective SIF (K_{eff}) is much higher than at 15°, causing greater stress intensities at the crack tip. The crack tip plastic zone also expands due to these intensified stress concentrations, promoting unstable growth. This results in rapid energy dissipation and a larger extent of structural damage, which is characteristic of brittle fracture under such high stress intensities. The analysis reveals that crack orientation has a significant impact on crack growth behavior and fracture mechanics. At 15°, stable crack growth is observed due to moderate stress intensities and gradual energy dissipation. Adhesion and toughness play a crucial role in resisting crack propagation, ensuring structural integrity. Conversely, at 60°, crack growth becomes unstable and accelerated due to higher stress intensities, mixed-mode fracture behavior, and rapid energy release (Table 5).

Table 5. Comparative Analysis of stable and unstable crack growth

Parameter	15° (Stable Growth)	60° (Unstable Growth)
Stress intensity factor	Moderate K_{eff}, K_I dominant	High K_{eff}, mixed-mode K_I+K_{II}
Fracture energy (G_c)	Reached slowly, stable growth	Exceeded quickly, unstable growth
Toughness utilization	Partial utilization	Full utilization, possible failure
Crack path	Linear propagation	Deviated and unstable
Plastic zone	Small and localized	Large, risk of yielding

6.2. Multiple Crack: A complex arrangement involving three or more interacting cracks (U2, S22)

In this scenario, three critical aspects related to crack formation and growth are discussed: displacement in the U2 direction, variations in stress distribution near the crack tip in the S22 direction, and crack opening mode. For this analysis, multiple cracks are predefined at angles of 60° and 120°. The obtained numerical modeling results are compared with those from the boundary element method (Abdollahipour, 2015), and the findings are interpreted accordingly. The

XFEM also plays a significant role in the numerical modeling of fracture mechanics problems, effectively predicting the formation and growth of both single and multiple cracks at various angles. The crack opening displacement and its propagation generally increase from 0^o to approximately 75^o Beyond 75^o, crack growth may cease, depending on the alignment between the applied loading path and the predefined crack angle. In such cases, cracks may form but not propagate further. When the predefined crack angle exceeds 90^o, the crack initially grows over a short path along the horizontal axis. As the crack angle approaches 90^o, stress distribution in the S22 direction decreases while adhesion forces increase. Crack propagation and crack opening displacement are directly influenced by the SIF and fracture toughness (K_{IC}). Figure 21 (a) and (b) illustrate the asymmetric crack growth and state of the multiple-crack formation at 60^o.

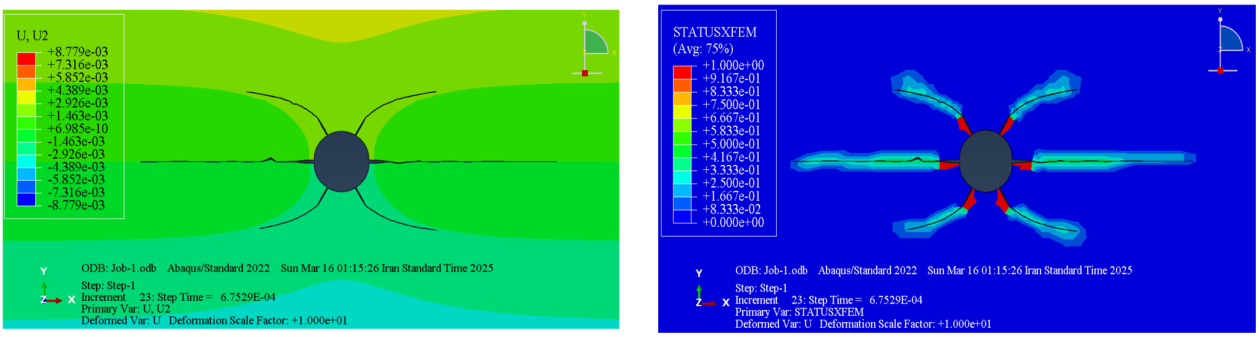

(a) **(b)**

Figure 21. Asymmetric crack growth and state of the multiple-crack formation at 60^o.

When the SIF reaches a critical threshold, cracks extend along a path determined by the stress field. The presence of multiple interacting cracks modifies the SIF distribution, affecting the direction and rate of crack growth. Strong adhesion between crack surfaces can resist propagation by reducing crack opening displacement, requiring higher applied stress to drive growth. A material's fracture toughness, which dictates its resistance to crack propagation, determines the energy needed for cracks to advance. Higher fracture toughness means greater energy is required. In multi-crack scenarios, local stress concentrations influence the critical stress intensity factor (K_{IC}), altering crack paths and velocities.

Figure 22 illustrates crack growth in a multiple-crack configuration at 120^o. The figures (a) and (b) show the most effective propagation pattern: the initial crack aligns with the horizontal axis, while two secondary cracks extend symmetrically at 120^o from it. This setup ensures stable growth and uniform crack opening, highlighting the importance of aligning the initial crack with the x-axis. The symmetrical secondary cracks promote balanced stress distribution and controlled fracture expansion, suggesting this configuration is ideal for predictable and efficient crack propagation. This is in contrast, the figures (c) and (d) depict a less favorable scenario where the initial crack aligns with the vertical axis, and secondary cracks extend at 120^o. Here, only the secondary cracks propagate, while the initial crack remains static, indicating an unbalanced fracture network due to suboptimal stress distribution. A similar pattern in figures (e) and (f) emerges when the initial crack is rotated 15^o from the vertical axis: the secondary cracks grow, but the initial crack does not. These findings underscore that improper initial crack orientation hinders balanced propagation, emphasizing the need to select an optimal angle for uniform and controlled fracture growth.

A 120^o fracture angle optimizes crack propagation by enhancing stress distribution, permeability, and fracture connectivity while potentially lowering breakdown pressure. This angle supports smoother crack growth, reduces deflection, and aligns fractures with the in-situ stress field, minimizing stress concentrations at crack tips for more uniform propagation. However, the extent of breakdown pressure reduction depends on rock anisotropy and stress conditions. The interaction of multiple fractures influences propagation through stress shadowing, where redistributed stress alters the SIFs of nearby cracks. This effect can either impede or promote growth, impacting fracture spacing, network complexity, fluid transport, and mechanical stability. Fracture toughness and energy demands are also affected, playing a key role in resource extraction and structural stability. This scenario underscores the

significance of crack interactions and their response to varying angles. The interplay of SIFs, adhesion, and fracture toughness governs crack initiation, propagation, and arrest.

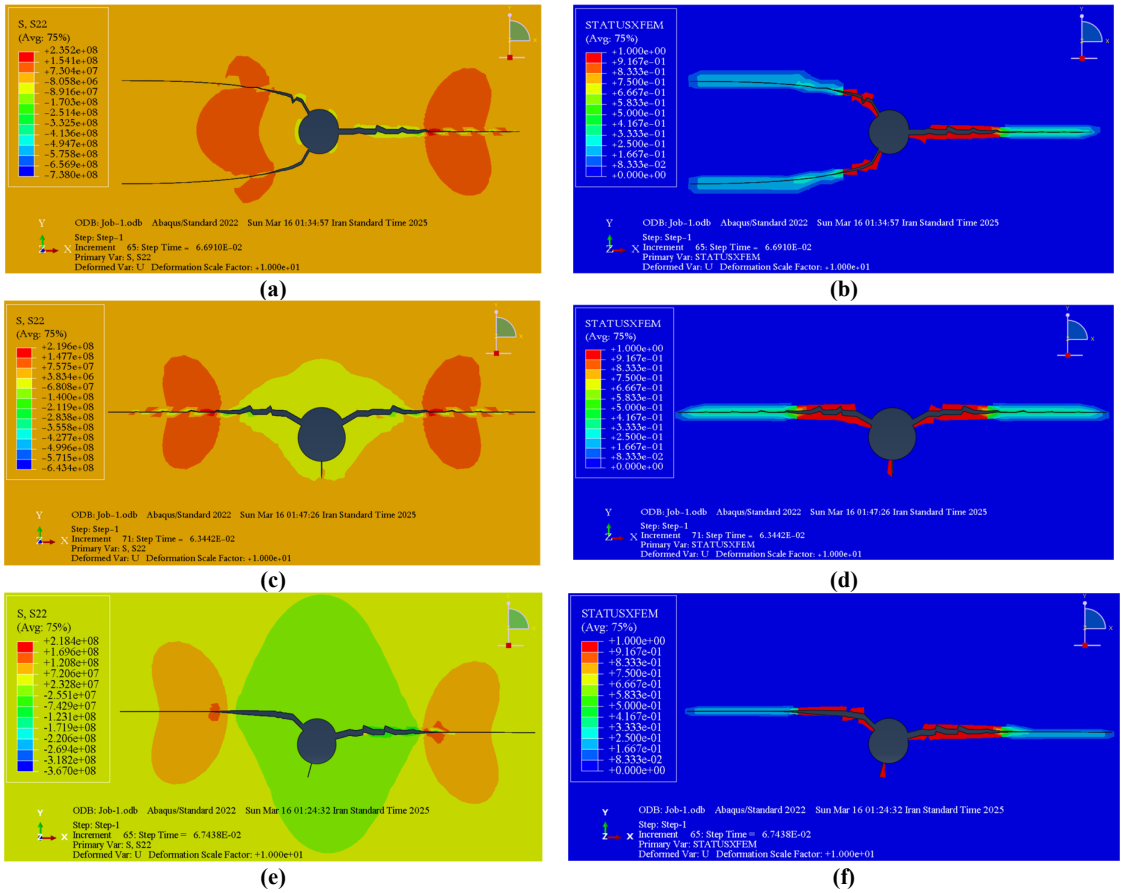

Figure 22. The state of multiple crack openings and propagation at a 120^{o} angle relative to the x and y axes.

6.3. Sensitivity Analysis

To assess the sensitivity of the model to variations in material properties, a parametric study was conducted by systematically altering the elastic modulus, shear modulus, and Poisson's ratio from the given values in Table 3. For the sensitivity analysis of the model, the parameter values are systematically varied relative to the baseline values provided in Table 6. Each parameter is tested once with a reduced value and once with an increased value compared to the initial values. Analysis revealed the following trends:

Table 6. Input parameters for sensitivity analysis.

Parameters	Values	Parameters	Values
E	38 GPa	E	30 GPa
G	16 MPa	G	10 MPa
v	0.4	v	0.25

If the elastic modulus (E), shear modulus (G), and Poisson's ratio (v) are lower than the given values, the crack aperture increases due to the reduced stiffness of the medium, allowing for greater deformation under the applied internal pressure ($P_{inj} = 30\ MPa$). In this case, the crack starts to propagate before the solution reaches the target increments and step time (Figure 23(b)). Conversely, if E, G, and Poisson's ratio (v) are higher than the given values, the crack aperture decreases, as the stiffer material resists deformation more effectively. In this case, when the solution reaches the target increment and step time, the crack does not start to propagate and remains unchanged (Figure 23 (a)). The target increment is 14, and the step time for the solution is assumed 4.0908e-02 second.

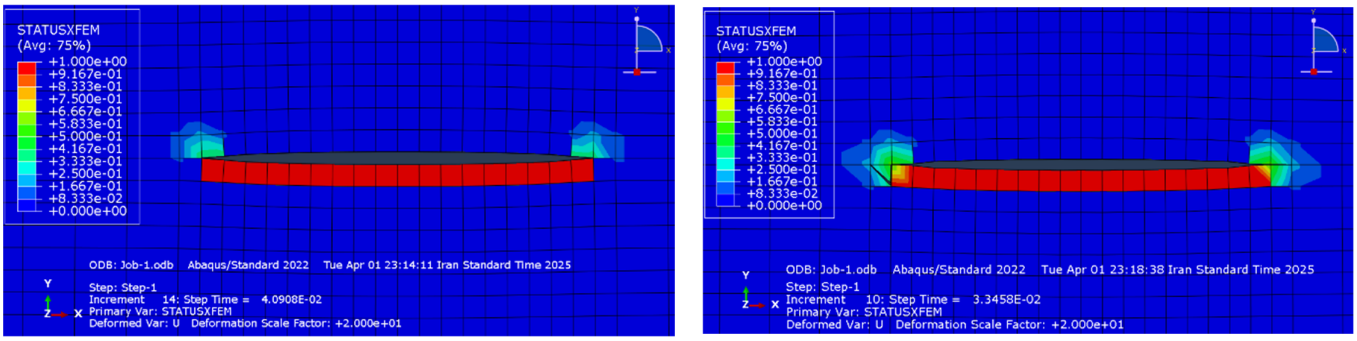

(a) **(b)**

Figure 23. Crack opening state for decreased (*E, G*, and *ν*) (a) and for increased (*E, G*, and *ν*) (b).

The stress distribution around the crack tip is significantly influenced by the elastic modulus, shear modulus, and Poisson's ratio, as these parameters determine the stiffness and deformation behavior of the material. A lower elastic modulus or shear modulus results in reduced stress concentration, a more diffused stress field, and an increased crack aperture due to the material's higher compliance. In contrast, higher values of these parameters cause stress to become more localized at the crack tip, increasing stress intensity and reducing crack opening. Poisson's ratio plays a smaller role, but its decrease slightly raises stress concentration and crack aperture, while its increase leads to better stress redistribution and a minor reduction in crack opening (Table 7). These findings highlight the necessity of accurately selecting material properties to ensure realistic fracture modeling and stress analysis.

Table 7. Effect of *E*, *G*, and ν variations on stress around the crack tip

Parameter change	Stress concentration near crack tip	Crack aperture	Stress field effect
↓ ***E* (lower stiffness)**	↓ Lower stress intensity (more diffused stress field)	↑ Larger	Stress spreads over a wider area
↑ ***E* (higher stiffness)**	↑ Higher stress intensity (more localized stress)	↓ Smaller	Stress concentrates at the crack tip
↓ ***G* (lower shear resistance)**	↓ Reduced shear resistance (more compliance)	↑ Larger	More significant Mode II (shear) effects
↑ ***G* (higher shear resistance)**	↑ Higher shear resistance (localized stress)	↓ Smaller	Increased stress concentration at the tip
↓ ***ν* (< 0.31)**	↑ Slight increase in stress near the tip	↑ Slightly larger	Reduced lateral contraction
↑ ***ν* (> 0.31)**	↓ Slight decrease in stress concentration	↓ Slightly smaller	Stress redistribution reduces intensity

7. Conclusions

Numerical simulation of crack propagation mechanisms due to hydraulic fracturing process is of at most importance in geomechanics. These mechanisms improve and enhance the understanding of crack growth behavior and fracture mechanics principles in hydraulic fracturing operations. In this study, the Extended Finite Element Method (XFEM) was employed to simulate crack growth, aperture opening, and crack propagation mechanism during hydraulic fracturing processes. The findings provide critical insights into the impact of crack orientation on propagation, with a focus on optimal crack angles that maximize permeability and improve fracture performance. By investigating various crack configurations, this research aims to refine the predictive models used in hydraulic fracturing, ultimately enhancing the accuracy of crack growth predictions and providing a better insight of the factors that influence fracture stability and propagation in subsurface formations. The key findings include:

- Crack orientation plays a crucial role in determining propagation characteristics. Lower-angle cracks tend to propagate more directly, while higher angles introduce complex mixed-mode behavior.
- Single crack scenarios at 0°, 15°, 30°, and 60° revealed that vertical displacement (U2) dominates crack opening, with increasing shear effects as the angle rises.

- The stability of crack growth varies with orientation, where cracks at smaller angles propagate more easily, whereas those approaching or exceeding 90º require additional stress to sustain growth.
- In multiple crack configurations at 60º and 120º, crack interaction effects significantly influenced growth behavior, stress redistribution, and fracture network development.
- Crack opening displacement increased with crack angle up to approximately 70º, beyond which propagation was sometimes hindered due to stress alignment with pre-existing fractures.
- The 120º crack angle proved to be the most effective for enhancing permeability and promoting stable crack propagation in hydraulic fracturing applications.
- A decrease in elastic modulus or shear modulus increases crack aperture due to reduced stiffness, while an increase in these parameters decreases crack aperture by limiting deformation.
- Poisson's ratio has a minor effect, with lower values slightly increasing crack aperture and higher values slightly reducing it, indicating a marginal stiffening effect.

This study confirms that XFEM is a reliable numerical method for modeling hydraulic fracture behavior, demonstrating how crack angles, stress distribution, and fracture mechanics parameters govern fracture evolution. However, limitations such as mesh dependency, convergence issues in complex crack geometries, and the exclusion of fluid flow interactions affect the accuracy of results. Future research should integrate fluid-structure interactions and anisotropic material properties to improve predictive accuracy in hydraulic fracturing simulations.

References

[1]. Lecampion, B., Desroches, J., Weng, X., Burghardt, J., & Brown, J. E. (2015). Evidence of the importance of near-wellbore fracture geometry from theory, lab and field experiments. *Society of Petroleum Engineers Journal*, (March), 539–557.

[2]. Wan, X. (2020). Coupled simulation of hydraulic fracturing production and refracturing for unconventional reservoirs [Doctoral dissertation].

[3]. Joshi, S. D. (2003). Cost/benefits of horizontal wells. *Society of Petroleum Engineers Journal*.

[4]. U.S. Energy Information Administration. (2019). International Energy Outlook.

[5]. Montgomery, C. T., et al. (2010). Hydraulic fracturing: An enduring technology. *Society of Petroleum Engineers*. Retrieved from

[6]. Australian Government. (2014). Hydraulic fracturing (fracking) techniques, including reporting requirements and governance arrangements.

[7]. Zielonka, M. G., Searles, K. H., Ning, J., & Buechler, S. R. (2014). Development and validation of fully-coupled hydraulic fracturing simulation capabilities. *SIMULIA Community Conference*, SCC2014, 1–31.

[8]. Guo, J., Zhao, X., Zhu, H., Zhang, X., & Pan, R. (2015). Numerical simulation of interaction of hydraulic fracture and natural fracture based on the cohesive zone finite element method. *Journal of Natural Gas Science and Engineering*, 25, 180–188.

[9]. Kim, J., & Moridis, G. J. (2015). Numerical analysis of fracture propagation during hydraulic fracturing operations in shale gas systems. *International Journal of Rock Mechanics and Mining Sciences*, 76, 127–137.

[10]. Ren, G., Jiang, J., & Younis, R. M. (2016). A fully coupled XFEM-EDFM model for multiphase flow and geomechanics in fractured tight gas reservoirs. *Procedia Computer Science*, 80, 1404–1415.

[11]. Yaylac, M., & Yaylac, M. (2016). The investigation crack problem through numerical analysis. *Structural Engineering and Mechanics*, 57(6), 1143–1157.

[12]. Abdollahipour, A., et al. (2018). Behavior of a hydraulic fracture in permeable formations. *Journal of Mining and Environment*, 9(4), 893–904.

[13]. Chen, X., Li, Y., Zhao, J., Xu, W., & Fu, D. (2018). Numerical investigation for simultaneous growth of hydraulic fractures in multiple horizontal wells. *Journal of Natural Gas Science and Engineering*, 51, 44–52.

[14]. Yaylaci, M., et al. (2022). Implementation of finite element and artificial neural network methods to analyze the contact problem of a functionally graded layer containing crack. *Steel and Composite Structures*, 45(4), 501–514.

[15]. Yaylaci, M. (2022). Simulate of edge and an internal crack problem and estimation of stress intensity factor through finite element method. Advances in Nano Research, 12(4), 405–416.

[16]. Yaylacı, M., Yaylacı, E. U., Özdemir, M. E., Öztürk, Ş., & Sesli, H. (2023). Vibration and buckling analyses of FGM beam with edge crack: Finite element and multilayer perceptron methods. *Steel and Composite Structures*, 46(4), 565–575.

[17]. Zeerak, M. R., Fatehi Marji, M., & Sanei, M. (2023). Investigating hydraulic fracture models for production enhancement of unconventional hydrocarbon reservoirs. *4th National Petroleum Geomechanics Conference*.

[18]. Fuyad, Sk. T. M., et al. (2024). Finite element analysis of ratcheting on beam under bending-bending loading conditions. *Structural Engineering and Mechanics*, 89(1), 23–34.

[19]. Fatehi Marji, M., Lak, M., & Sanei, M. (2023). The explosive fracturing technique analysis for highly low permeable reservoirs using analytical, displacement discontinuity and finite difference coupled method. *Journal of Petroleum Geotechnics*.

[20]. Benouis, A., et al. (2024). Finite element analysis of the behavior of elliptical cracks emanating from the orthopedic cement interface in total hip prostheses. *Structural Engineering and Mechanics*, 89(5), 539–547.

[21]. Yazdani, M., Fatehi Marji, M., Najafi, M., & Sanei, M. (2025). Simulating the hydraulic fracturing mechanism around the hydrocarbon wellbores with emphasizing its effects on the sand production. *Journal of Mining and Environment*, 16(1), 241–258.

[22]. Gerali, F. (2025). Hydraulic fracturing. Engineering and Technology History Wiki. Retrieved January 23, 2025,

[23]. Maiti, S. K. (2015). Determination of stress intensity factors. In Fracture Mechanics (pp. 102–151). Cambridge University Press.

[24]. Ritchie, R. O., & Liu, D. (2021). Introduction to fracture mechanics. *Elsevier.*

[25]. Singh, G., & Zimmerman, R. W. (2014). Modification of Griffith-McClintock-Walsh model for crack growth under compression to incorporate stick-slip along the crack faces. *International Journal of Rock Mechanics and Mining Sciences*, 72, 311–318.

[26]. Manouchehrian, A., & Fatehi Marji, M. (2012). Numerical analysis of confinement effect on crack propagation mechanism from a flaw in a pre-cracked rock under compression. *Acta Mechanica Sinica/Lixue Xuebao*, 28(5), 1389–1397.

[27]. McGinty, B. (2014). Loading modes (I, II, and III). Retrieved from https://www.fracturemechanics.org/modes123.html

[28]. Anderson, T. L. (2017). Fracture mechanics: Fundamentals and applications (4th ed.). Taylor & Francis.

[29]. Fatehi Marji, M. (2014). Rock fracture mechanics with displacement discontinuity method.

[30]. Feng, X., Fatehi Marji, M., & Abdullahipour, A. (2017). Rock mechanics and engineering. CRC Press.

[31]. Ali, A., & Rajakumar, C. (2004). The boundary element method: Applications in solids and structures (Vol. 2).

[32]. Moës, N., Dolbow, J., & Belytschko, T. (1999). A finite element method for crack growth without remeshing. *International Journal for Numerical Methods in Engineering*, 46(1), 131–150.

[33]. Sanei, M., Duran, O., Devloo, P. R. B., & Santos, E. S. R. (2022). Evaluation of the impact of strain-dependent permeability on reservoir productivity using iterative coupled reservoir geomechanical modeling. *Geomechanics and Geophysics for Geo-Energy and Geo-Resources*, 8(2), 1–25.

[34]. Li, H., Li, J., & Yuan, H. (2018). A review of the extended finite element method on macrocrack and microcrack growth simulations. *Theoretical and Applied Fracture Mechanics*, 97, 236–249.

[35]. Belytschko, T., Gracie, R., & Ventura, G. (2009). A review of extended/generalized finite element methods for material modeling. *Modelling and Simulation in Materials Science and Engineering*, 17(4), 043001.

[36]. Wu, L., Zhang, L. X., & Guo, Y. K. (2014). A review of the extended finite element for fracture analysis of structures. *Applied Mechanics and Mat*erials, 444–445, 96–102.

[37]. Dassault Systèmes. (n.d.). Modeling fracture and failure with Abaqus. Retrieved from https://www.technia.com/training/modeling-fracture-and-failure-in-abaqus/

[38]. Belytschko, T., Moës, N., Usui, S., & Parimi, C. (2001). Arbitrary discontinuities in finite elements. *International Journal for Numerical Methods in Engineering*, 50(4), 993–1013.

[39]. Wu, W.-L. (2004). Boundary element formulations for fracture mechanics problems [Doctoral dissertation]. University of Wollongong. Retrieved from http://ro.uow.edu.au/theses/253

[40]. Abdollahipour, A. (2015). Simulation of crack propagation mechanism in hydraulic fracturing process in oil reservoirs [Doctoral dissertation]. Yazd University.

[41]. Dassault Systèmes. Modeling fracture and failure with Abaqus.

[42]. Mohammadi, S. (2008). Extended finite element method: For fracture analysis of structures. Blackwell Publishing.

[43]. Economides, M. J., & Nolte, K. G. (2000). Reservoir stimulation (3rd ed.). Wiley.

[44]. Abass, H. H., Meadows, D. L., Brumley, J. L., Hedayati, S., & Venditto, J. J. (1995). Oriented perforations - A rock mechanics view. Proceedings of the Middle East Oil Show, 1, 13–27.

[45]. Portela, A., & Rooke, D. P. (1992). Dual boundary element analysis of crack growth. Computational Mechanics Publications. *International Journal of Fracture.* 55: 17-28,

انجمن مهندسی معدن ایران
نشریه مهندسی معدن و محیط زیست
نشانی نشریه: www.jme.shahroodut.ac.ir
دانشگاه صنعتی شاهرود

مدل‌سازی عددی شکست هیدرولیکی برای بررسی مکانیزم رشد ترک سنگ با استفاده از روش المان محدود توسعه‌یافته و اعتبارسنجی آن بر مبنای روش المان مرزی

محمدرضا زیرک[۱]، محمد فاتحی مرجی[۱*]، منوچهر صانعی[۱]، مهدی نجفی[۱] و ابوالفضل عبداللهی‌پور[۲]

۱. دانشکده مهندسی معدن و متالورژی، دانشگاه یزد، یزد، ایران
۲. دانشکده مهندسی معدن، دانشکدگان فنی، دانشگاه تهران، تهران، ایران

اطلاعات مقاله

تاریخ ارسال: ۲۰۲۵/۰۲/۲۷
تاریخ داوری: ۲۰۲۵/۰۴/۰۷
تاریخ پذیرش: ۲۰۲۵/۰۴/۲۰

DOI: 10.22044/jme.2025.15836.3047

کلمات کلیدی

روش المان محدود توسعه‌یافته
شکست هیدرولیکی
راستای رشد ترک
روش المان مرزی
مکانیک شکست سنگ

چکیده

روش المان محدود توسعه‌یافته (XFEM) یک روش محاسباتی برجسته برای مطالعه رشد ترک در سنگ‌ها است. زیرا می‌تواند مسیرهای پیچیده ترک و ناپیوستگی‌ها را بدون نیاز به مش‌بندی مجدد دقیق‌تر مدل‌سازی کند. در این زمینه روش XFEM به‌ویژه برای شبیه‌سازی توسعه شکست هیدرولیکی مناسب است. در این مطالعه، از روش XFEM به‌ویژه برای شبیه‌سازی شکست هیدرولیکی در حال گسترش استفاده شده است و برای بررسی شروع، انتشار و اندازه بازشدگی ترک در سازندهای سنگی به کار رفته است. با اعتبارسنجی از طریق رویکرد مبتنی بر روش المان مرزی (BEM) سه سناریو شامل ترک‌های منفرد (ناشی از شکست هیدرولیکی) در زوایای ۰، ۱۵، ۳۰ و ۶۰ درجه؛ رفتار جابجایی ترک در زوایای ۱۵ و ۶۰ درجه؛ و ترک‌های متعدد در زوایای ۶۰ و ۱۲۰ درجه برای تحلیل راستا و تعامل ترک‌ها مورد بررسی قرار گرفته است. جابجایی در راستای عمودی (U2) و توزیع تنش در اطراف نوک ترک در راستای S22 برای درک پارامترهای مکانیک شکست مورد بررسی قرار گرفته‌اند. یافته‌ها نشان می‌دهند که ترک‌ها در زوایای بالاتر، مانند ۱۲۰ درجه، انتشار بهتری دارند، در حالی که ترک‌ها در زوایای ۹۰ درجه یا بیشتر اغلب به تنش اضافی برای ادامه رشد، نیاز دارند. مقایسه نتایج XFEM و BEM قابلیت اطمینان روش عددی را تأیید می‌کند و سازگاری مناسبی در پیش‌بینی رفتار شکست در مواد سنگی را نشان می‌دهد. نتایج، بینش عمیق‌تری در مورد تکامل شکست، فاکتورهای شدت تنش و چقرمگی شکست در محیط‌های زمین‌شناختی فراهم می‌کنند. این شبیه‌سازی‌ها باعث پیشرفت مکانیک شکست محاسباتی گردیده و به بهینه‌سازی تکنیک‌های شکست هیدرولیکی برای بهبود کارایی و ایمنی در سازندهای زیرسطحی کمک می‌کنند. این مطالعه به مدل‌های دوبعدی و مواد ایزوتروپیک محدود است و ممکن است پیچیدگی‌های زیرسطحی ناهمسانگرد سه‌بعدی را در نظر نگیرد. تحقیقات آینده می‌توانند مدل‌های سه‌بعدی، ناهمسانگردی و اثرات فشار سیال/حرارتی را برای بهبود پیش‌بینی‌های رشد ترک بررسی کنند.

نویسنده مسئول مکاتبات: mfatehi@yazd.ac.ir (م. فاتحی مرجی)